Orbits of a Planet in a Protoplanetary Disk

A Report submitted

in partial fulfilment for the award of the Degree of

BACHELOR OF TECHNOLOGY

in

Physical Sciences

by

ATMA ANAND

pursued in

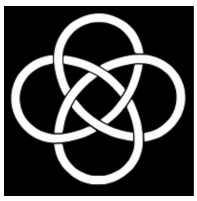

THE INTER-UNIVERSITY CENTRE FOR ASTRONOMY AND ASTROPHYSICS

to

INDIAN INSTITUTE OF SPACE SCIENCE AND TECHNOLOGY

Thiruvananthapuram

April 2016

Orbits of a Planet in a Protoplanetary Disk

A Report submitted

in partial fulfilment for the award of the Degree of

BACHELOR OF TECHNOLOGY

in

Physical Sciences

by

ATMA ANAND

pursued in

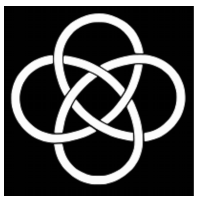

THE INTER-UNIVERSITY CENTRE FOR ASTRONOMY AND ASTROPHYSICS

to

INDIAN INSTITUTE OF SPACE SCIENCE AND TECHNOLOGY

Thiruvananthapuram

April 2016

अंतर–विश्वविद्यालय केंद्र : खगोलविज्ञान और खगोलभौतिकी IUCAA
Inter-University Centre for Astronomy and Astrophysics
An Autonomous Institution of the University Grants Commission

CERTIFICATE

This is to certify that the project report entitled **"Orbits of a Planet in a Protoplanetary Disk"** submitted by **Atma Anand** to the Indian Institute of Space Science and Technology, Thiruvananthapuram, in partial fulfillment for the award of the degree **B.Tech.** in **Physical Sciences**, is a bonafide record of the project work carried out by him under my supervision from **January 5, 2016** to **April 1, 2016**.

Dr. Kanak Saha
(Project Supervisor)
Assistant Professor
IUCAA, Pune

Dr. Somak Raychaudhury
Director
IUCAA, Pune

Place: Pune
April 2016

Dr. Anandmayee Tej
Countersign by Head of Department (ESS),
IIST, Trivandrum.

Mailing Address : IUCAA, Post Bag 4, Ganeshkhind, Pune - 411 007, India.
Location : Meghnad Saha Road, Pune University Campus, Pune - 411 007.
Phone : 020-2569 1414, 2560 4100 **I Fax :** +91-20-2560 4699
E-mail : root@iucaa.ernet.in
Uniform Resource Locator : http://www.iucaa.ernet.in/

DECLARATION

I declare that this report titled **"Orbits of a Planet in a Protoplanetary Disk"** submitted in partial fulfillment of the Degree of **Bachelor of Technology in Physical Sciences** is a record of original project work carried out by me under the supervision of **Dr. Kanak Saha**, and has not formed the basis for the award of any degree, diploma, fellowship or other titles in this or any other Institution or University of higher learning. In keeping with the ethical practice in reporting scientific information, due acknowledgements have been made wherever the findings of others have been cited.

Place: Thiruvananthapuram
April 2016

Name : Atma Anand
Roll No. : SC12B156

ACKNOWLEDGMENTS

I would like to express my sincere gratitude to my supervisor, **Dr. Kanak Saha** for his continuous support during my project period, for his patience, motivation, enthusiasm, and knowledge. I thank the IUCAA community for their warm hospitality and vibrant atmosphere which made working there a fun experience. I would also like to thank the Astronomy Group of the ESS Department of IIST for their support and guidance.

Name : Atma Anand

Roll No. : SC12B156

ABSTRACT

The effect of a protoplanetary disk, represented as a low-mass *Kuzmin disk* model, on the orbit of a planet around a host star is explored. In such a system, which is nearly Keplerian, the evolution time-scale is of the order of millions of years, while the revolution time-period is of the order of a few years. Hence, long term evolution of such systems need precise numerical schemes.

Since gravitationally bound systems almost always have a Hamiltonian which is conserved, symplectic methods of integration can be used which are faster and conserve the energy well, except for round-off errors (which grows linearly in general). Symplectic integrators were reviewed. The fourth order symplectic Forest-Ruth algorithm was used to solve the classical Keplerian two body problem and inspect its stability.

The protoplanetary disk is then introduced in the system. Motion is restricted to the $z = 0$ plane, and the two body problem is studied under further approximation of no motion of the host star. The mass and density of the disk were selected to be comparable to our Solar System, although the length-scale was selected to be quite large. The frequencies involved and the dynamics of the resultant orbit were examined using deviation from a circular orbit, Fourier decomposition, surface of section, and error analysis of integrals of motion.

For the traditional Kuzmin disk, it was found that the axis of the ellipse of motion precesses slowly due to added potential of the disc. The FFT gives the frequencies in the system to be the radial ($\approx$ azimuthal) and precession frequencies, as expected.

Next the effect due to perturbations from $m = 1$ mode asymmetric terms in the disc, were analysed. A shape function ($\log_e r$) was also added as a special case to the phase which introduces a spiral wave in the potential. The position and momentum space were found to be lopsided. There are subtle indications of the underlying disk potential in the phase space. The cases of both a constant asymmetry at all radii, and the asymmetry being localised primarily nearly the planet (Gaussian distribution) were considered. The

evolution of the system was found to be not easily generalisable and sensitive to the initial conditions, possibly as the angular momentum is no longer conserved. Although the orbit shows a quasi-periodic motion, the analysis hints that a suitable time dependence of the disk potential such that it subsequent disappears completely could cause a significant migration.

TABLE OF CONTENTS

LIST OF TABLES

LIST OF FIGURES

ABBREVIATIONS

L	Angular Momentum
AU	Astronomical Unit
ϵ	Asymmetry Parameter
φ	Azimuthal Angle (Cylindrical coordinates)
Ω	Azimuthal Frequency
e	Eccentricity of the orbit
FFT	Fast Fourier Transform
$\mathbb{H}$	Hamiltonian or Total Energy
K or T	Kinetic Energy
M_d	Mass of Disk
$M_\odot$	Mass of Sun
p	Momentum
q or **x**	Position
Φ or U	Potential
ϖ	Precession Frequency
κ	Radial Frequency
k	Radial Wave number
r	Radius
a	Disk scale length
§	Section
sma or a_o	Semi Major Axis of Planet
SOS	Surface of Section
t	Time
v	Velocity
Yrs	Years

CHAPTER 1

INTRODUCTION

The motivation for this study originates from one particular aspect of planet formation and evolution. As it is known, star formation begins with the collapse of a part of a molecular cloud which has reached a critical mass (or density). As this collapsing cloud or solar nebula becomes denser, collisions due to random motions of cloud particles originally present redistribute the velocity to favor the direction perpendicular to the nebula's net angular momentum and the radius vector. Conservation of angular momentum causes the rotation velocity to increase as the nebula contract which in turn causes the cloud to flatten out and take the form of a disk. The resulting partially collapsed structure has a stellar core surrounded by a disk which contains much of the angular momentum of the system, which is perpendicular to the disk. This *accretion disc* last for about 10^5 years following which the disk density drops due to accretion by the star or being blown away by stellar winds. This relatively long-lived (few million years) accretion disk continues to feed the star to a limit while also nurturing planetesimals and providing the environment for subsequent stages of planet formation. Being the precursor for planets, the disk is also called a *protoplanetary disk*.

Terrestrial planets are formed within this disk through continuous agglomeration of its material, growing sequentially into dust, rocks, planetesimals and protoplanets. As these bodies increase in mass, their growth and dynamics becomes increasingly dominated by gravitational interactions. Just prior to being completely lost by accretion or dissipation, the disk also provides a viscous medium partially responsible for planetary migration. Unmerged planetesimals may collide and form a *debris disk*, which can have lifetimes of GYrs if replenished. Some migration also occurs during the later stages as a result of gravitational scattering. The final structure of the system may be influenced by planet-planet interactions, until a configuration emerges which is dynamically stable over billions of years.[2]

This study seeks to see the effect of the protoplanetary disk (or possibly the debris disk) on the orbits of planets and to seek possible ways on how it may facilitate migration of terrestrial planets (specifically Type I migration).

1.1 Planetary Migration

Planetary migration occurs when a planet interacts with a disk of gas or planetesimals, resulting in the alteration of the planet's orbital parameters, in particular its semi-major

axis. Theoretical models of planet formation and evolution should be able to explain the most bizarre properties of exoplanets, as well as their statistical properties. But there are several observational discrepancies in the properties of planets and the distance from their host star at which they are found. These suggest that many planets were formed at a significantly different radii and then transfered to their current position via some form of migration. There are three major modes of planetary migration: gravitational scattering, tidal and disk migration.

Disk migration is brought about due to the disk-planet interaction. Depending on the property of the disk and mass of the planet, this migration is further divided into 3 types.[3]

- **Type 1** migration occurs for low-mass (terrestrial) planets whose interaction with the disk is weak enough to leave the disk structure almost undisturbed. This is true if the local exchange of angular momentum between the planet and the disk is negligible compared to the redistribution of angular momentum due to disk viscosity. The planet remains fully embedded within the gas disk and material is present at all resonant locations. Imbalance in the strength of the interaction with the spirals inside and outside (greater) the planet's orbit typically causes the planet to lose L_z and migrate inwards within the disk lifetime. Co-rotation torques by disk material typically raise L_z, causing outward migration. *Lindblad resonances* also exert considerable torque on the planet.[4]

- **Type 2** migration occurs for higher mass planets whose gravitational torques locally dominate angular momentum transport within the disk. This torque from the planet act to repel disk gas away from the orbit of the planet, opening an annular "gap" within the disk. Resonances close to the planet are severely depleted of material and contribute little or nothing to the total torque. However, material continues to enter the gap on the timescales of the accretion disk, moving the planet and gap inward. This mass flux torque is sensitive to local disk properties which acts on the planet, analogous to Type 1 migration.

- A kind of gas disk driven migration is sometimes referred to as runaway or *Type 3* migration, where large-scale vortices in the disk rapidly draw the planet in towards the star in a fraction of the orbital timescale.

Gravitational scattering by larger planets or by over-densities in the fluid of the protoplanetary disk can also lead to drastic migration.

Tidal migration occurs when to tides between the star and planet modify the semi-major axis and orbital eccentricity. Disk migration lasts about a million years until the gas dissipates, but tidal migration can continue for billions of years.

Observations of contemporary forming planetary systems have revealed that Jupiter-like planets (excluding hot-Jupiters) can be found in only 10% of cases. The further presence of Saturn make our System almost unique in known systems. The "Grand Track" model, based on the migration of Jupiter and the migration it may induce in turn, explains several key features of our solar system. The model with a Gaussian distribution of the asymmetry is attempted to simulate the effect of a forming Jupiter-like body on the orbit of the planet in question.

1.2 Problem Statement

The gravitational effect of the addition of a static protoplanetary disk on the orbit and long term evolution of the orbit of a (proto-)planet orbiting a host star is sought to be simulated and studied. The protoplanetary disk is modeled as a Kuzmin disk, the traditional variant of which has 2 parameters, the total disk mass (M_d) and a scale length (a). The evolution of the system has to computed by symplectic integration methods as the Hamiltonian remains conserved and other methods may introduce spurious effects (§2.1). Next, asymmetric perturbations corresponding to the $m = 1$ modes are added to the disk potential. Four cases of asymmetric perturbations were explored. While the effect of disks on the orbits of (proto-)planets is well documented, the effect of asymmetric perturbations to the disk in particular is not well studied.

The classical Kepler problem was solved over millions of years to test the robustness of the symplectic integration method. The orbitals elements found after the addition of the disk were examined directly or using surface of section, and Fourier decomposition. The addition of the traditional Kuzmin disk to the system being reasonably well understood was used as a testbed for the more complex asymmetric perturbations. The asymmetric disk cases employed can be divided into 4 subsections by the permutations of: a Gaussian form of the asymmetry or a constant asymmetry, and no radial dependence of the phase or a logarithmic phase term to mimic a spiral wave perturbations in the potential (or density).

In §2 the theoretical tools required for this study are reviewed. In §3 the effect of the addition of the traditional Kuzmin disk on the orbit of the planet is examined. In §4 the introduction of asymmetric perturbations in the Kuzmin disk is investigated. §5 consists of the conclusions, findings and future scope of this work. An appendix with the Fortran 95 implementation of the simulation can be found at the end. All plots have been plotted in *Gnuplot*, except for the contour plots which were made in *Python*.

CHAPTER 2

THEORETICAL BACKGROUND

The problem at hand focuses on systems having a central host star embedded at the center of a disk with a continuous mass distribution. It has been assumed that the system acts only gravitationally on the planet, although there is immense research which include additional effects due to the disk including hydrodynamics and back reactions on the disk[1]. The planet is in essence considered as a test particle. The Hamiltonian formalism to obtain the evolution of the system can be used as the energy always remains conserved. The general terminology, tools and methods used to treat such a system shall be discussed in this chapter.

2.1 Symplectic Integration

Our goal is to find the long term evolution of system which cannot be solved by analytical means. For this task the importance of a good integration scheme which is fast and precise cannot be overstated. The problem in this study is limited to simple cases in which the Hamiltonian is conserved. The evolution of a Hamiltonian system $[q(0), p(0)) \rightarrow (q(t), p(t)]$ is a symplectic transformation (canonical transformation, $dp \wedge dq = dp' \wedge dq'$). The numerical solution, therefore, obtained by a non-symplectic integrator will be spuriously damped or excited. (This was computationally verified for 1^{st} and 2^{nd} order methods.) There is no known advantage of using symplectic methods for systems for which the energy is not conserved.

Symplectic methods have several merits over traditional integrators [5], [6]:

- They have a property of area preserving (Fig. 2.1).
- The accumulated truncation error in variables increase linearly with the time instead of quadratic growth.
- Adaptive step-size is not required (and not recommended).
- The fourth order symplectic integrator requires 1 less force evaluation than RK4.

[1] For example see publications by Dr. John Papaloizou, Dr. Gordon Ogilvie, and Dr. Jeremy Goodman.

2.1.1 Symplectic Transformation

Given a system with n generalized coordinates $\mathbf{q}$, conjugated momenta $\mathbf{p}$ and Hamiltonian H,

$$\dot{q}_i = \frac{\partial H}{\partial p_i},\ and\ \dot{p}_i = -\frac{\partial H}{\partial q_i}, \quad i = 1, 2, ...n$$

For brevity, this can be expressed as

$$\mathbf{x} = \begin{pmatrix} \mathbf{q} \\ \mathbf{p} \end{pmatrix} \Rightarrow \dot{\mathbf{x}} = \mathbf{J}\frac{\partial H}{\partial \mathbf{x}}$$

where, $\mathbf{J} = \begin{pmatrix} \mathbb{O}_\mathbf{n} & \mathbb{I}_\mathbf{n} \\ -\mathbb{I}_\mathbf{n} & \mathbb{O}_\mathbf{n} \end{pmatrix}$, $\mathbb{O}_\mathbf{n}$ and $\mathbb{I}_\mathbf{n}$, are the the null and unity matrices of order n.

Let $\mathbf{y} = \mathbf{y}(\mathbf{x})$. Using invariance property of canonical transformation and chain rule:

$$\dot{\mathbf{y}} = \mathbf{J}\frac{\partial H}{\partial \mathbf{y}} = \mathbf{M}\mathbf{J}\mathbf{M}^t\frac{\partial H}{\partial \mathbf{y}}; \quad \text{with, } M_{ij} = \frac{\partial y_i}{\partial x_i}$$

Comparing the equations for $\dot{\mathbf{x}}$ and $\dot{\mathbf{y}}$ we can say that the transformation is canonical iff, the Jacobian matrix $\mathbf{M}$ satisfies the relation $\mathbf{M}\mathbf{J}\mathbf{M}^t = \mathbf{J}$.

2.1.2 Generating Symplectic Integrators

A Symplectic Integrator should mimic physical properties of the true flow of the continuous time problem (Fig. 2.1). Derivation of explicit schemes involve expansion of the *separable* Hamiltonian as Taylor series in different ways. All straightforward derivations of symplectic integrators assume that the *Hamiltonian is separable* into functions of exclusively the coordinates or the momenta. Any cross terms lead to complications in applying the symplectic method. A time step involves sub-steps depending on the order, but each sub-step or their combinations is symplectic by itself ($\mathbf{M}\mathbf{J}\mathbf{M}^t = \mathbf{J}$). (See [5], [6])

The conventional methods of obtaining symplectic integration schemes are listed below.

1. Generating Function, W (of *von-Zeipel* Type)

$$\mathbf{p} = \frac{\partial W}{\partial \mathbf{q}},\ and\ \mathbf{q}' = \frac{\partial W}{\partial \mathbf{p}'}$$

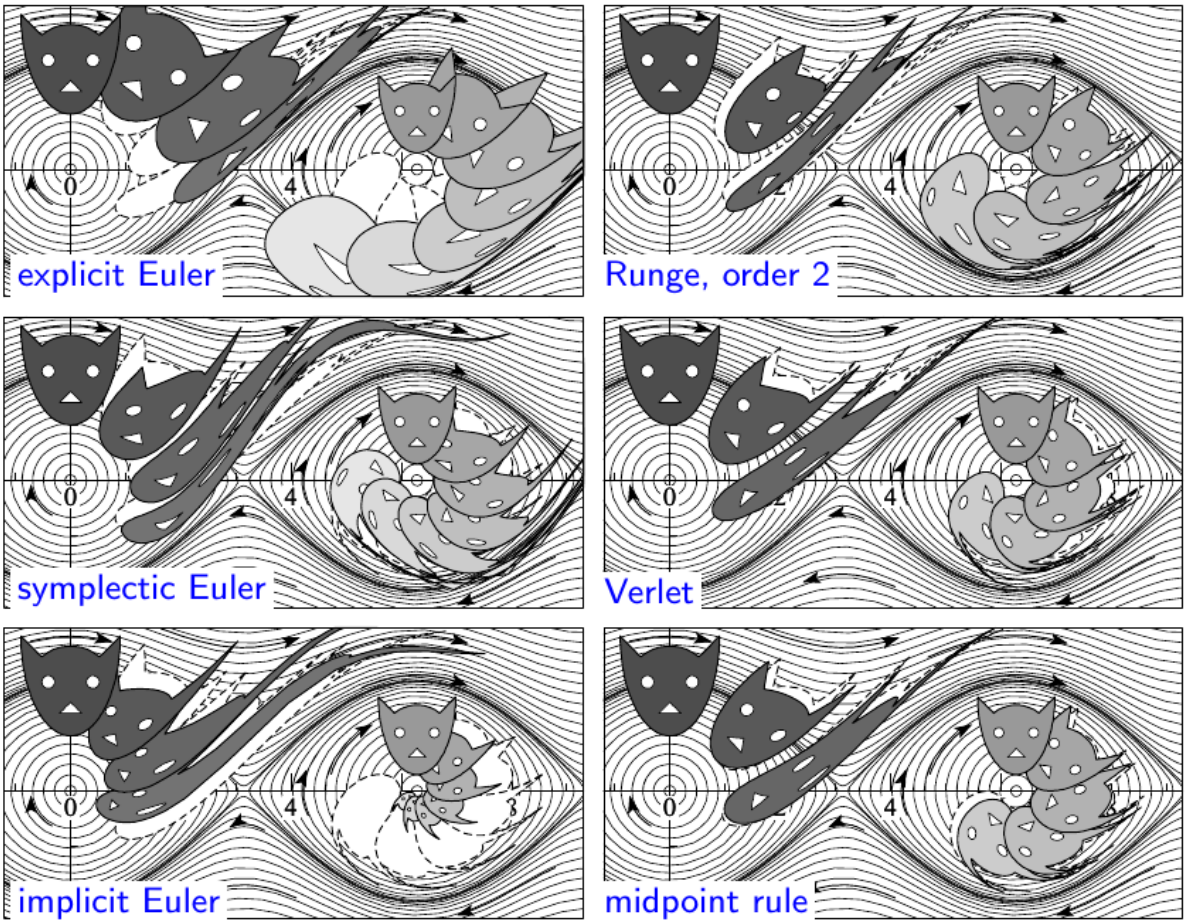

Figure 2.1: Comparison of lower order numerical integration methods for the pendulum problem. [1, Pg. 176]

It is desirable that the cat faces overlap the white area made by the dashed lines, which represents the true flow of the system.

The function W, in principle can be expanded to n^{th} order

$$W = qp' + \tau H(p, q') + \frac{\tau^2}{2} H_{p'} H_q + ...$$

After which the above differentiation can be carried out to obtain $\mathbf{q}'$ and $\mathbf{p}'$ from the initial $\mathbf{q}$ and $\mathbf{p}$. This method appears to combine all sub-steps into a single more intensive step.

2. Poisson Bracket as an operator ($H = T + U$).
   The Hamiltonian H is split into Kinetic (T) and Potential (U) terms. From the definition of a Poisson bracket and the Hamiltonian formalism, we have

$$\frac{dz}{dt} = \{z, H(z)\} = D_H\, z$$

Performing a definite integral from $t = 0$ to τ, we get

$$\Rightarrow z(\tau) = \exp(\tau D_H) z(0)$$

The operator D_H can then be split

$$z(\tau) = \left[\prod_{i=1}^{k} \exp(c_i \tau D_T) \exp(d_i \tau D_U) \right] z(0)$$

The integer k determines the order. Note that the approximation is introduced as D_T and D_U do not commute in general.

3. Group theory and other methods are also used which utilize the special properties of the Hamiltonian. See §5 of Forest and Ruth (1990)[7] for an example.

If in a small time step h the integration is performed so that it is accurate through order h^k, then the method is referred to as a k^{th}-order integration method. The kind of differential equations of interest here are those derivable from a Hamiltonian. The exact solution of such a system of differential equations leads to a symplectic map from the initial conditions to the present state of the system. However, a characteristic feature of most high-order ($k > 2$) integration methods is that they are not exactly symplectic. A sign of this is that the determinant of the Jacobian of the transformation for one time step differs slightly from unity, and thus the system will be damped or excited artificially. In many situations the notable features in the solutions appear only after long integration time or large numbers of iterations. These spurious artifacts may lead to misleading results. Symplectic integrators of various orders have been obtained to help overcome this problem, at least till the limit of truncation error.

2.1.2.1 Explicit Symplectic Integrator of 4th order

Given a Hamiltonian which can be separated into functions of **p** and **q** (Kinetic and Potential energy), $\mathcal{H}(\mathbf{p}, \mathbf{q}) = T(\mathbf{p}) + U(\mathbf{q})$, Forest-Ruth SI4 is [7]:

$$\begin{aligned} \mathbf{q}_{i+1} &= \mathbf{q}_i + c_i \tau \frac{dT}{d\mathbf{p}}(\mathbf{p}_i) \\ \mathbf{p}_{i+1} &= \mathbf{p}_i - d_i \tau \frac{dU}{d\mathbf{q}}(\mathbf{q}_{i+1}) \end{aligned} \tag{2.1}$$

where, $c_1 = c_4 = \frac{1}{2(2-2^{1/3})}$, $c_2 = c_3 = \frac{1-2^{1/3}}{2(2-2^{1/3})}$,

$$d_1 = d_3 = \frac{1}{2-2^{1/3}}\,, \quad d_2 = -\frac{2^{1/3}}{2-2^{1/3}}, \quad d_4 = 0.$$

The numerical coefficients (c_i, d_i), are determined so that the sequence of canonical transformations $(q, p) \rightarrow (q', p')$ coincides with the Taylor expansion of the solution up to the order of τ^4. The 8 equations thus obtained are quite long and usually solved computationally. Note that some steps have a $-ve$ time interval. The method was tested on the classical Kepler problem and found to be quite stable for problems where the energy is conserved and there are no close encounters (Fig. 2.2).

The error in integrals in this method appears to be limited by just the machine roundoff or truncation errors at double floating-point precision. An attempt to reduce the roundoff error using the algorithm suggested by Earn (1994)[8] was not found to be advantageous for the computation time increment in the problem considered.

This algorithm has been used to solve the equations of motion throughout this document. This was also compared with the 4^{th} order Runge-Kutta method. While there was no clear winner in terms of error of the integrals for the step size, timescale and the systems chosen, the SI4 method is expected to handle coarser time-steps, have relative errors oscillating about zero, and is about 25% **faster**.

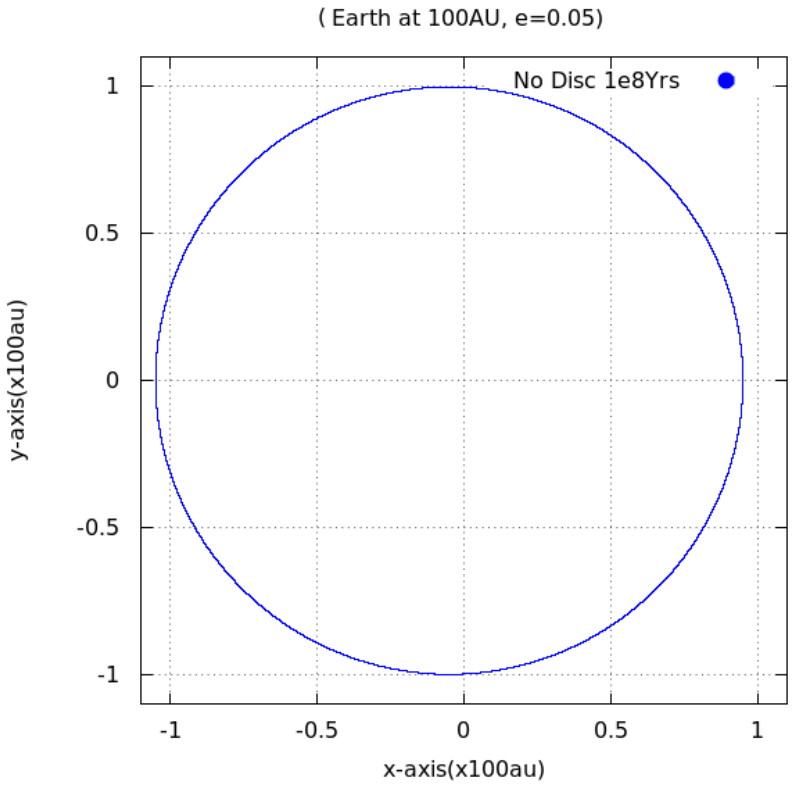

Figure 2.2: Planet Orbit for the Classical Kepler problem (100 MYr).
The mass of the planet and star were taken to be same as Earth and Sun. No deviation is visible.

2.2 Integrals of Motion

A *constant of motion* in a given force field is any function $C(\mathbf{x}, \mathbf{v}; t)$ of the phase-space coordinates and time that is constant along stellar orbits, i.e., if the position and velocity along an orbit are given by $\mathbf{x}(t)$ and $\mathbf{v}(t) = \mathrm{d}\mathbf{x}/\mathrm{d}t$, then[9, §3.1.1]

$$C[\mathbf{x}(t_1), \mathbf{v}(t_1); t_1] = C[\mathbf{x}(t_2), \mathbf{v}(t_2); t_2]$$

for any t_1 and t_2.

An *integral of motion*, $I(\mathbf{x}, \mathbf{v})$, is any function of the phase-space coordinates alone that is constant along an orbit:

$$I[\mathbf{x}(t_1), \mathbf{v}(t_1)] = I[\mathbf{x}(t_2), \mathbf{v}(t_2)] \tag{2.2}$$

While every integral of motion is a constant of the motion, the converse is not true.

Integrals that do not affect the phase-space distribution of an orbit, i.e., they fail to restrict the orbit to a smaller (in most cases, a dimension lesser) subspace of the permissible phase space, are called *non-isolating integrals*. All other integrals are called **isolating integrals**. Energy (E) and each component of angular momentum **(L)** are some parameters which, if conserved, individually confine stars to a five-dimensional region in the phase space. Isolating integrals are of great practical and theoretical importance, whereas non-isolating integrals are of essentially no value for our purpose.

In this study, the Energy (E) is an isolating integral in all cases. Further, as there is no motion in the z direction, $L_x = L_y = 0$ are isolating integrals themselves (restrict motion to only the $z = 0$ plane). L_z is an isolating integral if the force acting on the body is purely central. Purely Keplerian systems (Force $\propto 1/r^2$) also support a 5^{th} integral, the $Laplace - Runge - Lenz$ vector[10] which is closely related to the eccentricity vector.

2.3 Frequencies

Orbits are characterized by certain timescales and their corresponding frequencies.

The circular or azimuthal velocity V_c is the velocity with which the body moves in order for the centripetal acceleration to be equal to the radial acceleration.

The frequency linked with the circular velocity ($\vec{V_c} = \vec{\Omega} \times \vec{r}$ in general) is the circular or azimuthal frequency $\Omega(r)$.

The radial period T_r is the time required for the star to travel from apocenter (r_1) to

pericenter (r_2) and back.

The azimuthal period T_φ is the time corresponding to the mean angular speed of the particle Ω ($= 2\pi/T_\varphi$), *i.e.* the time it takes to complete a revolution.

The radial or epicyclic frequency $\kappa(r)$ is the frequency of radial oscillations from the apocenter to the pericenter.

The difference between the circular and radial frequencies is the precession frequency ϖ. It is a measure of the rate at which the line of apsides rotates about the center.

We have the following relations from the above definitions:[9]

$$\begin{aligned} \Omega^2(r) &= \frac{1}{r}\frac{\partial \Phi}{\partial r} \\ \kappa^2(r) &= 4\Omega^2 + r\frac{\partial \Omega^2}{\partial r} \\ \varpi(r) &= \Omega(r) - \kappa(r) \end{aligned} \tag{2.3}$$

$$T_r = 2\int_{r_1}^{r_2} \frac{\mathrm{d}r}{\sqrt{2[E-\Phi(r)] - L^2/r^2}} = \frac{2\pi}{\kappa} \tag{2.4}$$

In traveling from pericenter to apocenter and back, the azimuthal angle φ increases by an amount $\Delta\varphi$

$$\Delta\varphi = 2\int_{r_1}^{r_2} \frac{\mathrm{d}\varphi}{\mathrm{d}r}\mathrm{d}r = 2L\int_{r_1}^{r_2} \frac{\mathrm{d}r}{r^2\sqrt{2[E-\Phi(r)] - L^2/r^2}}$$

$$T_\varphi = \frac{2\pi}{|\Delta\varphi|}T_r = \frac{2\pi}{\Omega}$$

For a purely Keplerian system the radial (κ) and azimuthal (Ω) frequencies are equal and there is no precession. However, due to the addition of a Kuzmin disc the radial frequency becomes marginally higher and the system precesses very slowly. See Table 3.1) for the values of frequencies in the traditional Kuzmin disk.

The *Fourier transform* of the right elements of the orbit phase space should give peak values at these frequencies (Fig. 3.4).

2.4 Surface of Section

A surface of section (SOS), also called a Poincarè section, is a way of presenting a trajectory in $n-$dimensional phase space in a $(n-1)-$dimensional subspace.[2] By picking one phase element constant and plotting the values of the other elements each time the selected element has the desired value, an intersection surface is obtained. For real orbits, $n = 6$, but only 2D plots can be visualized. Hence, at least 2 integrals of motion (usually $E,$ or some L component) are required to bring the dimension down to 4 (say $x,\ v_x,\ y,\ v_y$), after which we choose a "slice" or plane on the 4D space (say $y = 0$) and plot the other coordinate and momentum (then $x,\ v_x$) when the conjugate momentum is either $+ve$ **or** $-ve$ (here both have been used). The obtained SOS are uniquely determined for that Energy and L_z as orbits in phase space do not intersect. A SOS plot shows orbits having the same energy but different initial conditions (such as **L**)[9, §3.2.2].

This is typically done by keeping a track of the trajectory during integration. However, for systems restricted to $2D$ motion, we can have alternate means of obtaining the SOS **if** L_z is also conserved. Fig. 3.6 shows the SOS for the trajectory in Fig. 3.3.

[2]For a good visual representation of surface of section for common orbits in galaxies, visit the Java applet at: http://burro.astr.cwru.edu/JavaLab/SOSweb/backgrnd.html

CHAPTER 3

ADDED KUZMIN DISK

Kuzmin (1956) found the potential of an infinitesimally razor-thin disk with Plummer's potential in the plane of the disk. It is also often referred to as "Toomre's model 1" because it became widely known only after Toomre unknowingly re-derived it in 1963. The protoplanetary disk was chosen in the form of a Kuzmin model as the potential and density of a Kuzmin disk is nearly constant (or varies slowly) at small radii (compared to the scale length) while the density falls sharply as r^{-3} at large radii. It has the added advantage of being a well familiar model, being used to model disks in several kind of systems.

Given a disk mass M_d and scale length a, the resulting Kuzmin disk has the following attributes [9].

1. Surface Density (Σ_d):

$$\Sigma_d(r) = \frac{aM_d}{2\pi(r^2+a^2)^{3/2}} \tag{3.1}$$

2. Enclosed mass

$$M_{in}(R) = M_d\left(1 - \frac{a}{\sqrt{R^2+a^2}}\right) \tag{3.2}$$

3. Potential (Φ_d):

$$\Phi_d(r,z) = -\frac{GM_d}{\sqrt{r^2+(a+|\,z\,|)^2}} \tag{3.3}$$

   (Here we always consider $z = 0$.)

4. Radial κ, Azimuthal Ω, and Precession $\dot{\tilde{\omega}}$ Frequencies, considering a star of mass $M_\odot$ at the center of the disk. As $\Omega \approx \kappa$, the resultant system is nearly-Keplerian even with a $10^{-1}M_\odot$ disc (see Table 3.1).[11]

$$\begin{aligned}
\Omega^2(r) &= \frac{1}{r}\frac{\partial\Phi}{\partial r} = \frac{GM_\odot}{r^3} + \frac{GM_d}{(r^2+a^2)^{3/2}} \\
\kappa^2(r) &= 4\Omega^2 + r\frac{\partial\Omega^2}{\partial r} = \frac{GM_\odot}{r^3} + GM_d\frac{4a^2+r^2}{(r^2+a^2)^{5/2}} \\
\varpi(r) &= \Omega(r) - \kappa(r) \approx \sqrt{\frac{r^3}{GM_\odot}}\frac{3}{2}\frac{GM_d}{(r^2+a^2)^{5/2}}
\end{aligned} \tag{3.4}$$

Table 3.1: Comparison of Frequency and Timescales for different Kuzmin Disc masses at $100AU$ with $a = 2.5 \times 10^{-3} pc$.

Mass(M_d)	Ω (rad/s; Years)	κ (rad/s; Years)	ϖ (rad/s; Years)	Period (Yrs)
0	6.283627×10^{-3}	6.283627×10^{-3}	0	999.92
	999.9297	999.9297	—	
0.1	6.285794×10^{-3}	6.292057×10^{-3}	-6.26289×10^{-6}	994.79
	999.5849	998.5899	1.003239×10^{6}	
0.001	6.283648×10^{-3}	6.283711×10^{-3}	-6.26812×10^{-8}	999.87
	999.9262	999.9163	1.00240264×10^{8}	

We introduce this disk as the background, such that the center of mass of the disk coincides with the star. As the disk is axis-symmetric, there is no force on the star due to the disk.

3.1 Selection of Disk Parameters

The solar system standard is used to form a basis to assign the disk parameters. The solar neighbourhood gas density is generally quoted as $= 0.04 M_\odot \, pc^{-3}$. Approximating the scale height of the thin disk at the galactic solar radius to be about $\sim 200pc$ so that the mass density can be considered constant, we get the density of the medium in solar neighbourhood to be around $8 M_\odot \, pc^{-2}$.

We adjust the parameters such that $M_d \sim$ present mass of solar system without the sun $(0.01 - 0.001 M_\odot)$ and $\Sigma_d(r = a) \sim 8 M_\odot \, pc^{-2}$. As there are 2 conditions and 2 parameters of the disk, a simultaneous equation system can also be made to obtain the disk parameters.

The parameters found suitable for the disk are: $a = 2.5 \times 10^{-3} pc,$ and $M_d = 10^{-3} M_\odot$. Such a disk is nearly Keplerian, implying $\kappa(r) \approx \Omega(r)$ (Table 3.1).

Note that mass of the solar system without the sun is about $1.4 \times 10^{-3} M_\odot$, although formation theories suggest the initial proto-planetary disk could be as massive as $10^{-2} M_\odot$. For the traditional Kuzmin disk, the $10^{-1} M_\odot$ model was found to give almost the same effect as its lighter counterpart on the system, but at a $\sim 1/100^{th}$ of the evolution timescale (hence lower computation time). This may be attributed to the negligible effect that even the $10^{-1} M_\odot$ model has on the total potential of the system. Fig. 3.1 shows the equi-potential contours for the $10^{-3} M_\odot$ Kuzmin Disk.

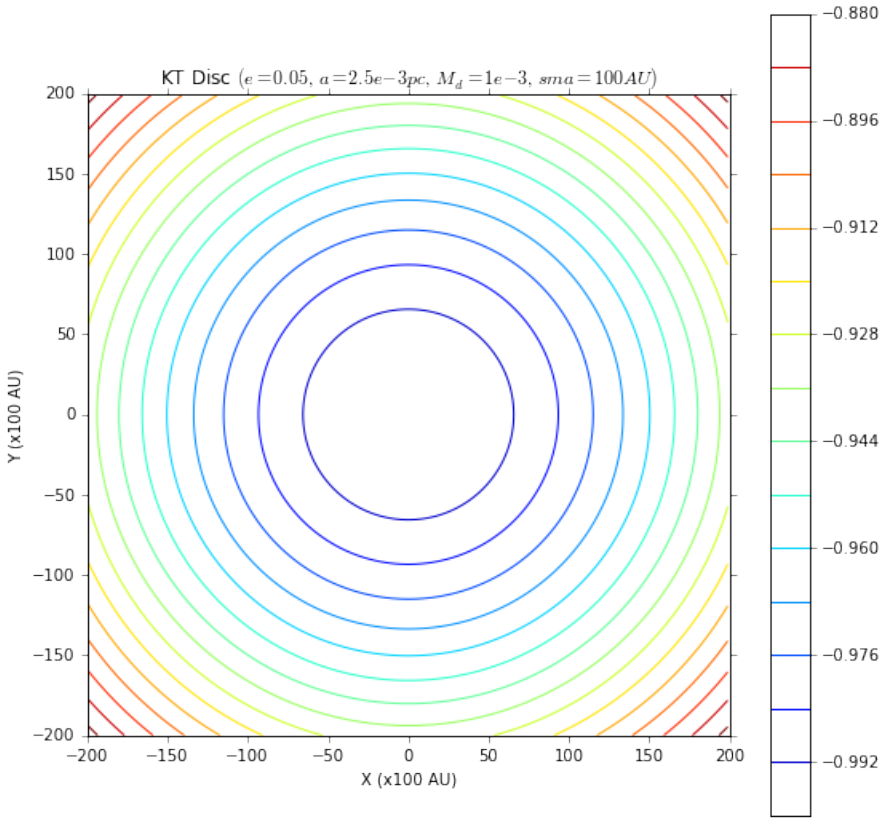

Figure 3.1: Equipotential contours generated by a $10^{-3}M_{\odot}$ Kuzmin Disk. The potential is scaled to be -1 at the origin (maxima).

3.2 Equations of Motion

Without loss of generality, we can assume mass of the planet as unity so that, $\dot{\mathbf{x}} = \mathbf{v} = \mathbf{p}$. The Hamiltonian for the planet with the added Kuzmin disc is then given by:

$$\mathcal{H}(\mathbf{x}, \mathbf{p}) = \frac{1}{2}\mathbf{p}^2 - \frac{GM_{\odot}}{|\mathbf{x}|} - \frac{GM_d}{\sqrt{|\mathbf{x}|^2 + a^2}} \tag{3.5}$$

Following the Hamiltonian formalism to obtain the dynamics of the system, we get:

$$\begin{aligned} \dot{\mathbf{p}} &= -\frac{d\mathbb{H}}{d\mathbf{q}} = -\nabla\Phi_{total} = \left(-\frac{GM_{\odot}}{|\mathbf{x}|^2} - \frac{GM_d|\mathbf{x}|}{(|\mathbf{x}|^2 + a^2)^{3/2}}\right)\hat{r} \\ \dot{\mathbf{x}} &= \frac{d\mathbb{H}}{d\mathbf{p}} = \mathbf{p} \end{aligned} \tag{3.6}$$

Although it is easier to do analytic calculations for a disk-like system in the polar (or cylindrical) coordinate system, it is often much more convenient to use *Cartesian coordinates for computation*. As motion is limited to the $x\,y$ plane, the above equations then change to:

$$\dot{x} = v_x \tag{3.7}$$

$$\dot{y} = v_y \tag{3.8}$$

$$\ddot{x} = -\frac{GM_\odot\, x}{r^3} - \frac{GM_d\, x}{(r^2+a^2)^{3/2}}$$

$$\ddot{y} = -\frac{GM_\odot\, y}{r^3} - \frac{GM_d\, y}{(r^2+a^2)^{3/2}} \tag{3.9}$$

where, $r = \sqrt{x^2+y^2}$

3.3 Implementation

The equations of motion were formulated by the Hamiltonian formalism (Eqn. 3.6) and 4^{th} order symplectic algorithm (Eqn. 2.1) was implemented in FORTRAN 95 (See Appendix 1 for code). RK4 method and lower order symplectic methods (Euler, Verlet, Velocity-Verlet) were also tried but SI4 was found to be superior.

3.3.1 Approximations

The no disk case needs no approximation. It is very easy to observe the elliptic motion of both the star and the planet under the influence of each other's gravitational force.

However, in the presence of the Kuzmin disk at the origin, the acceleration of the center of mass, $\ddot{R}_{cm} \neq 0$. This occurs as the motion of planet causes the star to shift from the origin. Though the motion of the host star is inversely proportional to the planet mass ratio, it is sufficient for the resultant acceleration of the disk on the center of mass of the star-planet system to become non zero. This causes R_{cm} to go in a periodic motion of small amplitude (Fig. 3.2, for earth mass planet and sun mass star).

When we **neglect the star's motion**, the change in force ($\Delta F_\odot$) experienced by the planet of mass$= m_p$ is $\Delta F_\odot \sim 2\frac{M_\odot}{m_p}\frac{GM_\odot}{r^2}$. We can assume the star to be much more massive than the planet to justify this assumption. An important reason to make the star much more massive is to neglect motion of the center of mass which could be a *source of asymmetry* in our otherwise assumed symmetric potential.

Hence, we assume the star and disk remain stationary at the origin and the only motion is of the planet. This is also acceptable as an order of magnitude numerical evaluation of the forces reveal that: $Force\ due\ to\ star >>> Force\ due\ to\ disk >> \Delta F_\odot$.

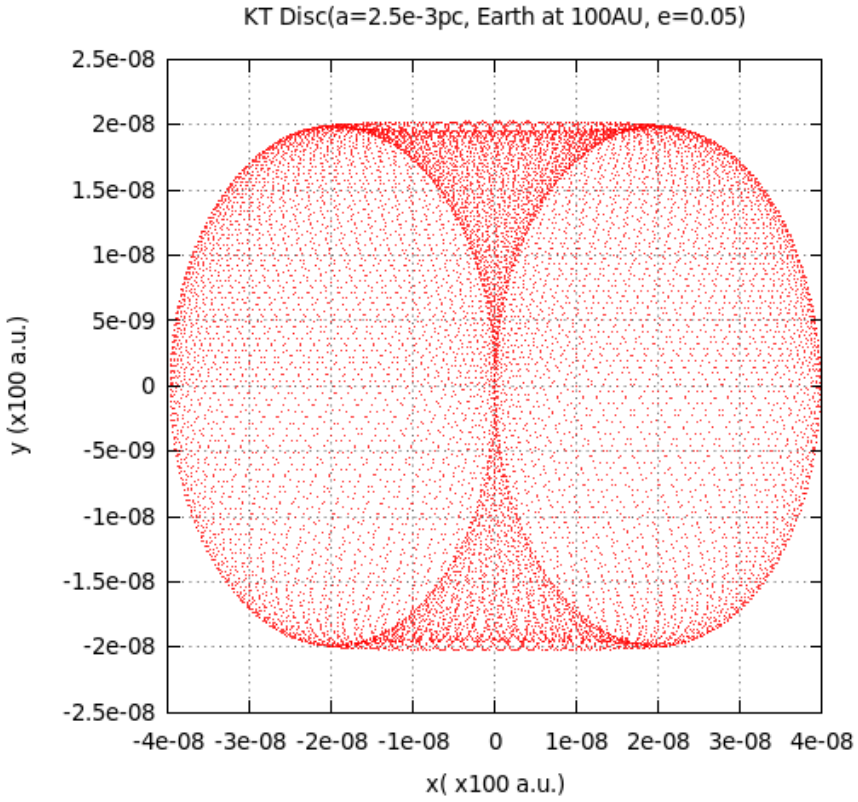

Figure 3.2: Motion of the star-planet barycenter due to the $10^{-3}M_{\odot}$ Kuzmin Disk.

Note that though this assumption does not cause any visible problems in this case, it might lead to noticeable errors once asymmetric perturbations are added to the disk.

3.3.2 Initial Condition and Limits

The planet was placed in a orbit of eccentricity 0.05 and semi-major axis $100AU$ and its motion around a sun mass star embedded in the Kuzmin disk was studied with a time step of 0.1 years (0.01 years time-step was also tried). Initial condition (Cartesian coordinates) is perigee with v_p found from vis-viva equation. Position, velocity, $\Delta E/E$, $\Delta L_z/L_z$, eccentricity, and deviation from perfect circle was sampled every 100 yrs (due to high amount of data generated). The initial eccentricity is such chosen as most planets are observed to have low but non-zero eccentricities.

Due to differences in magnitudes of units involved, the quantities were made dimensionless (arbitrarily) such that:

$$GM_{\odot} \equiv 1, \text{ and } 32\,km\,s^{-1} \equiv 2 \text{ (in dimensionless units)}$$

giving us the scaling parameters, $r_c,\ t_c,\ v_c$ for position, time and velocity respectively as:

$$v_c = 16 \times 10^3 (m\, s^{-1}),\ r_c = \frac{GM_\odot}{v_c^2}\,(m),\ t_c = \frac{r_c}{v_c}\,(s)$$

Time limit of integration was typically kept as the smaller of $0.2\,Gyr$ or a few precession timescale.

Note that theoretically, a coarser time-step could have been used for the symplectic algorithm at least till the symmetric disk case, however as the code executes is less than 20 minutes even for $0.2Gyrs$ for the most complex case of this study and there is a possibility of unwanted effects as the problem gets more complex, we stick to a $10^{-1}yrs$ time-step.

3.3.3 Observations

The results obtained from the above can be seen in the following plots. Fig. 3.3 shows the (proto-)planet orbit and its deviation from a perfect circle. The maximum deviation from the unit circle (with radius = semi-major axis to be precise) was found to be $\sim e\,a_0$, where e is the eccentricity and a_0 is the semi-major axis. Fig. 3.4 shows the Fourier decomposition of the r component of the deviation which gives peaks at κ and its harmonics (which may be artifacts). Fig. 3.5 shows the relative energy and angular momentum errors for the orbit (note that they are always opposite in sign), which appear to be due to truncation and possibly the numerical scheme used. Fig. 3.6 shows the surface of section of orbits in a $10^{-3}M_\odot$ Kuzmin disk having different initial angular momenta (but at the same energy). The velocity/momentum space was found to be topologically similar to the position space (ranging in absolute value from $2833.4\,m/s$ to $3131.7\,m/s$). The eccentricity was found to change minutely (in the 5^{th} decimal place) over the timescale used and hence is not shown.

3.4 Discussion

This chapter focuses on orbits of a planet when a $10^{-3}M_\odot$ or $10^{-1}M_\odot$ Kuzmin disc with $a = 2.5 \times 10^{-3} pc$ is added as the background potential along with the host star.

The *visible* integrals are E, and $\mathbf{L}$ (all 3 components). As the value of φ is insufficient to exactly determine the value of r, a 5^{th} integral should be absent, although the deviation from a constant value is expected to be small. The Laplace-Rung-Lenz vector is conserved only for purely central forces ($F \propto r^{-2}$), *i.e.*, in the strict absence of the disk. The $-\nabla\Phi_d$ contribution, though small, violates that condition, although the force remains purely

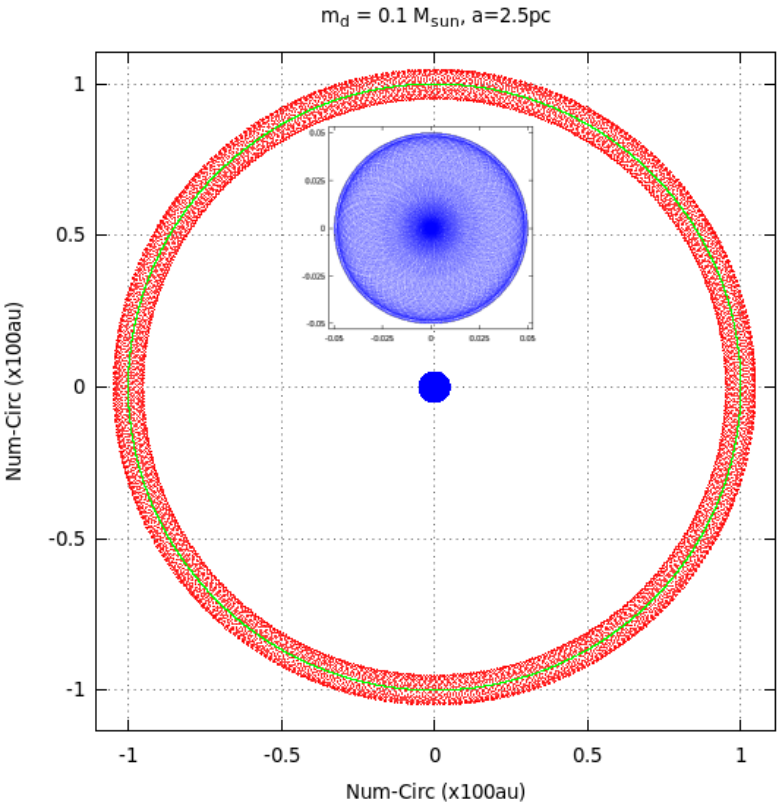

Figure 3.3: Planet orbit (red) and deviation (blue) from circular orbit (green). Initial eccentricity is 0.05. Star and disk are fixed.

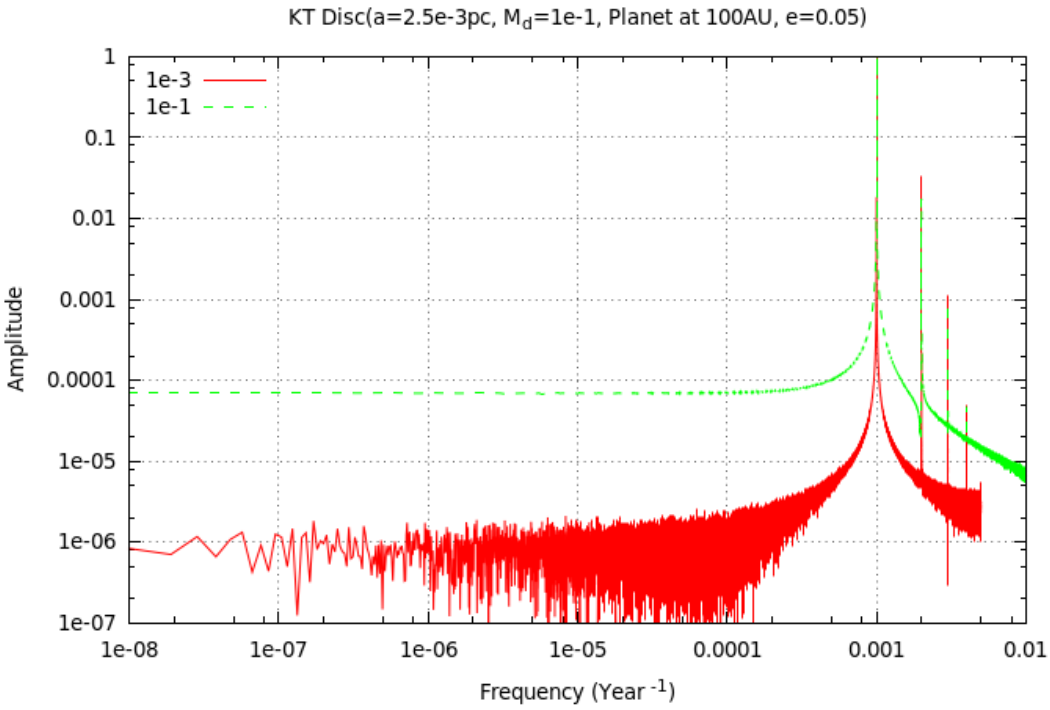

Figure 3.4: FFT of r vs t.

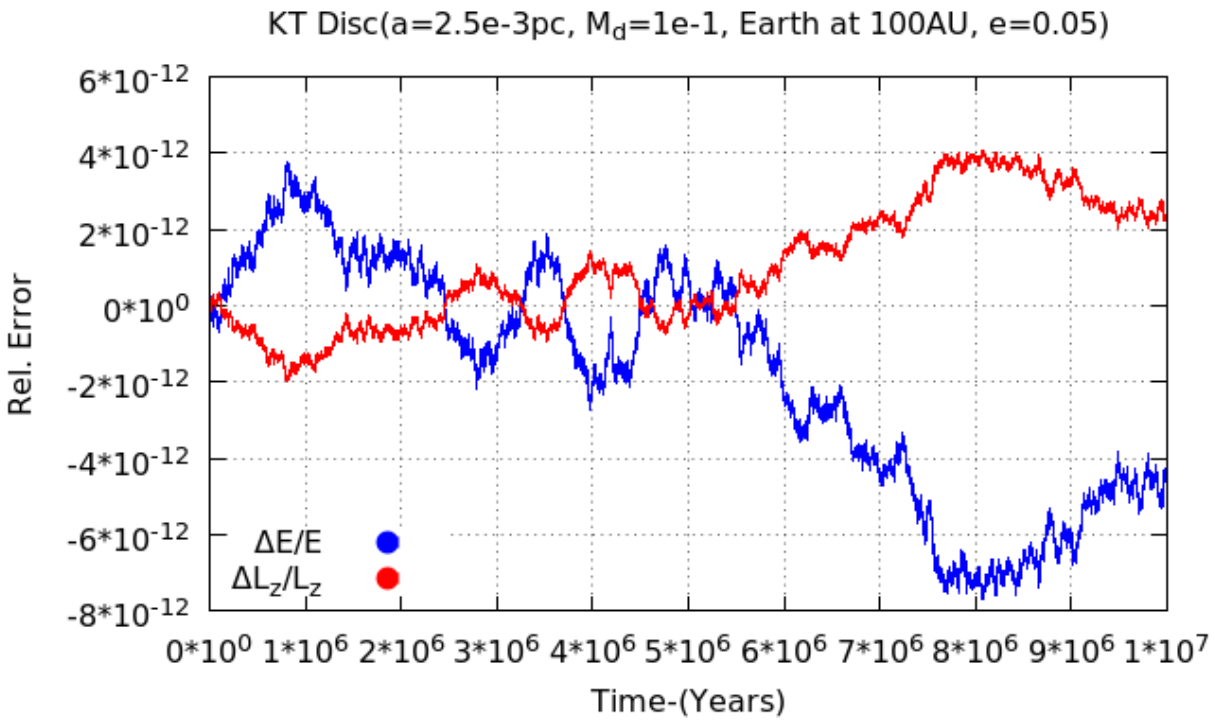

Figure 3.5: Relative deviation of Energy and L_z from initial value.

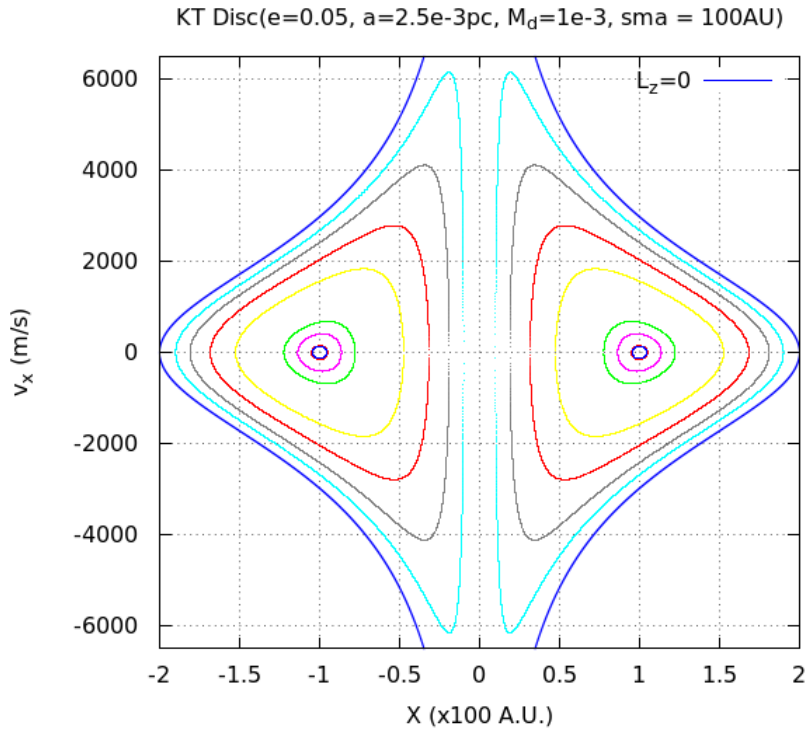

Figure 3.6: Surface of Section for added $10^{-3}M_{\odot}$ Kuzmin disk.
$L_z = 0$ gives an upper limit of v_r at given r.

radial. Further, as azimuthal and radial time-periods are non-commensurable, the orbit

does not close upon itself resulting in a loop orbit which eventually passes through all points in the annular region between the apogee and perigee (Fig. 3.3). This can also be viewed as precession of the axis of the ellipse determined by the initial conditions. This also means that *circular orbits cannot differentiate* appreciably between this case, and a central object which is as massive as the mass of part of the disc enclosed within the orbit (which is tiny) and the host star, although very minor deviation in from the circular orbit are present.

A Fourier transform can be done to get insight into frequencies involved in the system. The FFT of radial deviation of the trajectory from a circle having radius equal to semi-major axis gives peaks at $\kappa(\sim \Omega)$ (Fig. 3.4) and its harmonics (decreasing amplitudes which maybe due to numerical artifacts), and as well as at the precession frequency (ϖ) when just x or y component of motion is considered. The amplitude of the deviation from circular orbit is the product of the eccentricity and semi major axis. The Poincaré surface of section of the phase space ($y = 0,\ x = 0\ or\ \varphi = 0$, all are equivalent here) forms a closed curve (Fig. 3.6), further indicating the presence of loop orbits. This is a *Quasi-periodic orbit* meaning that though the orbit is not strictly periodic, it is still well-behaved and regular. The errors in integrals ($E,\ L_z$) are still consistent with those expected from roundoff (Fig. 3.5).

An attempt was made to fit of the last points of the trajectory with an elliptic orbit but it was not conclusive to determine any change in eccentricity, focus, or semi-major axis of the orbits. However, a scalar multiple of the LRL vector, the *eccentricity vector*, **e** gives the eccentricity and direction of the line of apsides.

$$\mathbf{e} = \frac{\mathbf{v} \times \mathbf{L}}{GM_\odot} - \hat{r} = \left(\frac{v^2}{GM_\odot} - \frac{1}{r}\right)\mathbf{r} - \frac{\mathbf{r} \cdot \mathbf{v}}{GM_\odot}\mathbf{v}$$

Computation of the eccentricity vector shows minor fluctuation in the eccentricity for this case. The semi-major axis (a_0) is expected to be constant (or very nearly constant), as the total energy depends on the approximate value of the semi-major axis and is an integral. Thus, we conclude that the dynamics of this case are reasonable well understood and can be predicted given suitable initial conditions.

CHAPTER 4

ASYMMETRIC KUZMIN DISK

Asymmetric perturbations corresponding solely to the $m = 1$ modes were introduced in the potential directly, thus bypassing the need to find the asymmetric perturbations to the surface density in an initial study. However, the surface density may be required for fine tuning the forces, in particular the force resulting from the motion of the host star due to back reaction from the disk.

The form of the perturbation used is

$$\begin{aligned}\Phi_{1,d}(r,\varphi,z) &= \Phi_d(r,z)\,\epsilon(r)\,\cos\{\varphi + f(r)\}\exp(-\,|k_0\,z|) \\ &= -\frac{GM_d}{\sqrt{r^2+(a+|\,z|)^2}}\,\epsilon(r)\,\cos\{\varphi + f(r)\}\exp(-\,|k_0\,z|)\end{aligned} \tag{4.1}$$

where, r is taken to be in A.U.

The total potential in the $z = 0$ plane is then given by

$$\Phi_{Total}(r,\varphi) = -\frac{GM_\odot}{r} - \frac{GM_d}{\sqrt{r^2+a^2}}\,[1+\epsilon(r)\,\cos\{\varphi + f(r)\}] \tag{4.2}$$

The frequencies, Radial κ, Azimuthal Ω, Precession ϖ, then simply change according to Equation 2.3.

The *asymmetry parameter* ϵ, itself can be a function of radius or be a constant. Both the constant epsilon case and the case where $\epsilon(r)$ varies as a normal distribution (Equation 4.8) with r and additional parameters $r_\epsilon,\ r_\sigma$ were used for the simulation. The $\epsilon(r)$ which varies as a normal distribution with a *small* r_σ serves as a good representation of another forming (massive) planet and the effect of such a structure on the orbit of the planet can then be studied.

$f(r)$ is the *shape function* $-$ a phase term. The sign convention is taken for galaxies which are mostly found to have trailing spirals as they help facilitate the disk material transfer angular momentum outwards and spiral in towards the center (which usually has a compact object), increasing the stability of the system[9]. Again, two forms of the shape function were considered, the trivial case of $f(r) = 0$ and the spiral density wave form $f(r) = \frac{1}{2}\log_e(r)$. The equi-potential contours for some of these cases can be seen in Fig. 4.1 to Fig. 4.3.

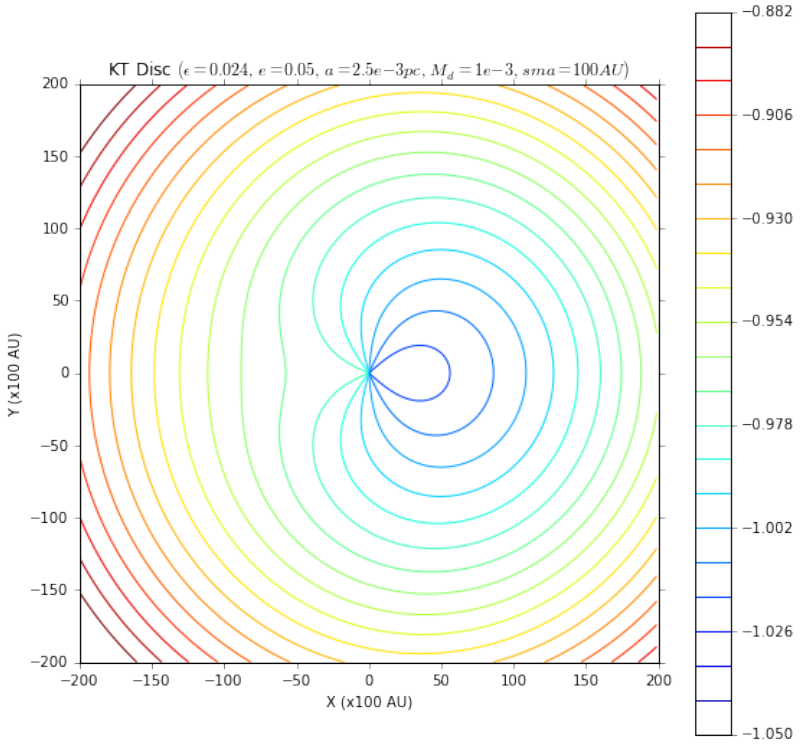

Figure 4.1: Equipotential contours generated by a $10^{-3}M_{\odot}$ Kuzmin Disk with constant asymmetry parameter $\epsilon = 0.024$ and $f(r) = 0$.

The potential is scaled to be -1 at the origin with $\epsilon = 0$

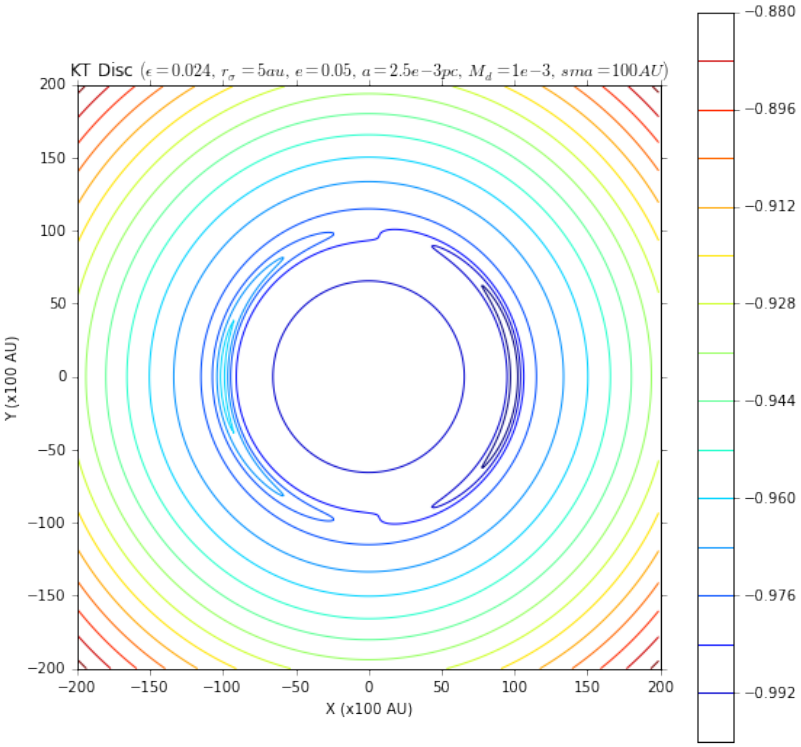

Figure 4.2: Equipotential contours generated by a $10^{-3}M_{\odot}$ Kuzmin Disk with Gaussian asymmetry with $r_\epsilon = 100au,\ r_\sigma = 5au,\ \epsilon_0 = 0.024$ and $f(r) = 0$.

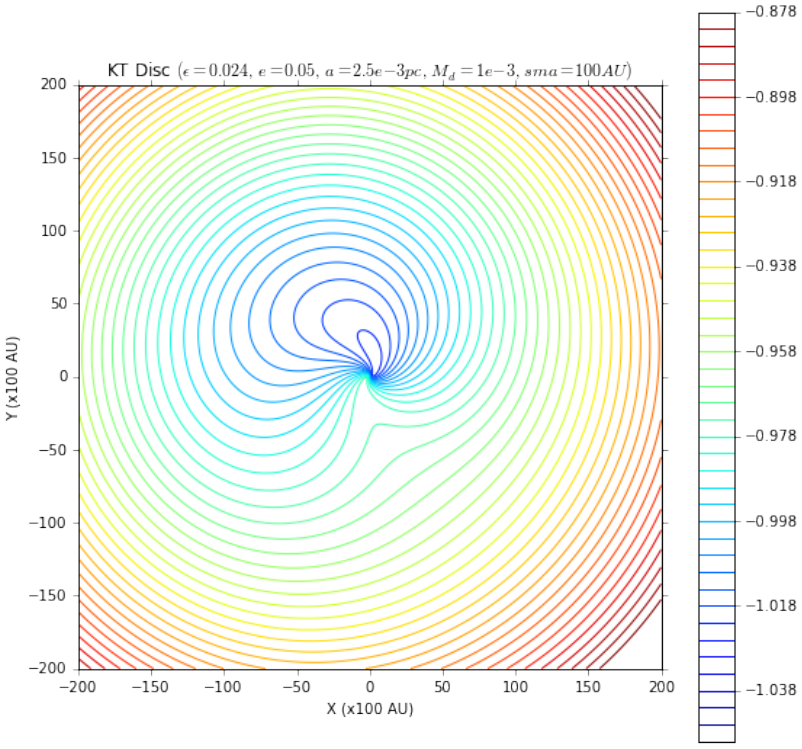

Figure 4.3: Equipotential contours generated by a $10^{-3}M_{\odot}$ Kuzmin Disk with constant asymmetry parameter $\epsilon = 0.024$ and logarithmic shape function.

4.1 Equations of Motion

Without loss of generality, we can again assume mass of the planet as unity so that, $\dot{\mathbf{x}} = \mathbf{v} = \mathbf{p}$.

The Hamiltonian for the planet with the added asymmetric Kuzmin disc is then given by:

$$\mathcal{H}(\mathbf{x}, \mathbf{p}) = \frac{1}{2}\mathbf{p}^2 - \frac{GM_{\odot}}{r} - \frac{GM_d}{\sqrt{r^2 + a^2}}(1 + \epsilon\, \cos\{\varphi + f(r)\}) \tag{4.3}$$

where, $|\mathbf{x}| = r$ and $\varphi = \tan^{-1}(y/x)$ Following the Hamiltonian formalism to obtain the evolution of the system, we get:

$$\begin{aligned}
\dot{\mathbf{p}} =& -\nabla\Phi_{total} = \left(-\frac{GM_{\odot}}{r^2} - \frac{GM_d\, r}{(r^2 + a^2)^{3/2}}(1 + \epsilon\, \cos\{\varphi + f(r)\}) - \frac{GM_d}{\sqrt{r^2 + a^2}} \times \right. \\
& \left. \left(\frac{\mathrm{d}[\epsilon(r)\, \cos\{\varphi + f(r)\}]}{\mathrm{d}r}\right)\right)\hat{r} - \left(\frac{GM_d\, \epsilon(r)}{r\sqrt{r^2 + a^2}} \sin\{\varphi + f(r)\}\right)\hat{\theta} \\
\dot{\mathbf{x}} =& \frac{\mathrm{d}\mathbb{H}}{\mathrm{d}\mathbf{p}} = \mathbf{p}
\end{aligned} \tag{4.4}$$

As Cartesian coordinates are preferred for computation, the above equations have to be changed depending on the case.

It is apparent that the force in this case is no longer purely radial and the tangential term leads to a torque (τ) on the planet which will vary the angular momentum ($z-$component) over time.

$$\vec{\tau}(r,\varphi) = \vec{r} \times \vec{F} = -\frac{GM_d}{\sqrt{r^2+a^2}}\epsilon(r)\sin(\varphi + f(r))\,\hat{z} \tag{4.5}$$

Spiral structure (shape function) produce spiral gravitational field, which exerts torques and transfers angular momentum from one part of the disk to another. This leads to the secular evolution of the disk (not accounted in this study) and may influence bodies embedded in the disk. The z-component of the torque exerted on the disk material outside the cylinder of radius R for the case with $f(r) = \frac{1}{2}\log_e(r)$ is ([9, §6.1.5], [12, §3])

$$C_z(R) = \frac{1}{4G}\frac{k}{|k_0|}\epsilon^2(R)\Phi_d^2(R) \tag{4.6}$$

where, the radial wave number $k = df/dr$, $k_0 = \sqrt{k^2 + R^{-2}}$ and $\Phi_d(R)$ is the potential of the traditional Kuzmin disk at radius R. It is easy to see that C_z increases from 0 at the origin, peaks near a, and then asymptotically converges of 0 at ∞ for the constant ϵ case. C_z behaves approximately as the asymmetry distribution for the Gaussian $\epsilon(r)$ case.

4.2 Implementation

The equations of motion were formulated by the Hamiltonian formalism (Eqn. 4.4) and 4^{th} Order symplectic algorithm was implemented in FORTRAN 95 (See Appendix 1).

As there are two $\epsilon(r)$ and two $f(r)$, there are a total of 4 cases of $\mathrm{d}[\epsilon(r)\,\cos\{\varphi + f(r)\}]/\mathrm{d}r$. The derivative of ϵ and $f(r)$ w.r.t. r will be shown separately and chain rule can simply be applied according to the case to get the full equation of motion.

1. $\epsilon(r) = \epsilon$

$$\frac{\mathrm{d}\epsilon}{\mathrm{d}r} = 0 \tag{4.7}$$

2. $\epsilon(r) = \epsilon_0\,\exp\left(-\frac{(r-r_\epsilon)^2}{r_\sigma^2}\right)$

$$\frac{\mathrm{d}\epsilon(r)}{\mathrm{d}r} = -2\frac{\epsilon(r)\,(r-r_\epsilon)}{r_\sigma^2} \tag{4.8}$$

3. $f(r) = 0 \Rightarrow \mathrm{d}f/\mathrm{d}r = 0$

4. $f(r) = \frac{1}{2}\log_e(r)$

$$\frac{\mathrm{d}f(r)}{\mathrm{d}r} = \frac{1}{2r} \tag{4.9}$$

The most general form of the equations of motion, i.e. for the Gaussian $\epsilon(r)$ then reads:

$$\dot{\mathbf{p}} = \left(-\frac{GM_\odot}{r^2} - \frac{GM_d\, r}{(r^2+a^2)^{3/2}}(1+\epsilon\,\cos\{\varphi + 0.5\,\log_e(r)\}) + \frac{GM_d}{\sqrt{r^2+a^2}}\times \right.$$
$$\left.\left(\frac{\epsilon(r)}{2r}\sin\{\varphi+0.5\,\log_e(r)\} - 2\frac{\epsilon(r)\,(r-r_\epsilon)}{r_\sigma^2}\right)\right)\hat{r} - \left(\frac{GM_d\,\epsilon(r)}{r\,\sqrt{r^2+a^2}}\sin\{\varphi+0.5\,\log_e(r)\}\right)\hat{\theta} \tag{4.10}$$

4.2.1 Initial Condition and Limits

The motion of the host star is again neglected for the sake of simplicity. The planet's initial condition is kept the same, a orbit of eccentricity 0.05 and semi-major axis $100AU$. While the energy alters very slightly due to the asymmetric component of the potential, the difference is about 10^{-4} times less than the total energy in the added traditional Kuzmin disk case and can be neglected. The planet moves around a sun mass star embedded in the asymmetric Kuzmin disks of the types mentioned above. Initial condition (Cartesian coordinates) is perigee with v_p found from vis-viva equation. Position, velocity, $\Delta E/E$, $\Delta L_z/L_z$, and eccentricity were sampled every 100 years.

Due to differences in magnitudes of units involved, the quantities were made dimensionless (arbitrarily) as in the traditional Kuzmin disk case such that:

$$GM_\odot \equiv 1, \text{ and } 32\,km\,s^{-1} \equiv 2 \text{ (in dimensionless unit)}$$

again giving the scaling parameters, $r_c,\ t_c,\ v_c$ as:

$$v_c = 16\times 10^3 (m\,s^{-1}),\ r_c = \frac{GM_\odot}{v_c^2}\,(m),\ t_c = \frac{r_c}{v_c}\,(s)$$

Time limit of integration was typically kept as the smaller of $0.2\,Gyr$ or a few precession timescale. The time step used was 0.1 years.

4.2.2 Observations

The plots for selected runs of this case can be seen below from Fig. 4.4 to Fig. 4.15. The Table 4.1 shows the extremum values of $\Delta L_z/L_z$ and its large scale oscillation timescale for cases with zero shape function. Minor oscillations (over a radial time period) were

Table 4.1: Summary for added asymmetric Kuzmin disk with $f(r) = 0$.

ϵ_0	r_σ	r_ϵ	$(\Delta L_z/L_z)_{max}$	$(\Delta L_z/L_z)_{max}$	ϖ (MYrs)
0.01	15	85	0	-0.0182	33.4
0.01	15	100	0	-0.028	75
0.01	15	115	0	-0.072	58
0.02	15	85	0	-0.026	22
0.02	15	100	0	-0.054	71
0.02	15	115	0	-0.121	60
0.024	15	85	0	-0.027	19
0.024	15	100	0	-0.065	71
0.024	15	115	0	-0.141	61
0.024	5	95	0	-0.0009	1.82
0.024	5	100	0	-0.028	1.02
0.024	5	105	0	-0.0019	2
0.024	1	99	0.00125	0	3.7
0.024	1	100	0	-0.0052	102
0.024	1	101	0.00125	0	3.2
0.024	∞	–	0	-0.75	187
0.02	∞	–	0	-0.35	130

found to be $\approx 1000Yrs$ in all cases, though minute differences may be present. For the case with spiral density wave and Gaussian form of the asymmetry, the $\Delta L_z/L_z$ was found to oscillate appreciably from $+ve$ to $-ve$ values, although the $-ve$ cycle dominates. The $\Delta L_z/L_{z,0}$ is important to observe as it relates directly of the change of orbital radius and eccentricity from the initial value. For the $f(r) = 0$ cases, the orbital space was generally found to have a symmetry about some line $\perp$ to the x-axis while the velocity space was always evidently lopsided.

4.3 Discussion

The orbits of a planet with an added asymmetric Kuzmin disc as the background potential along with the host star, is not subject to easy generalizations as can be seen from the above plots. All models were based on $a = 2.5 \times 10^{-3} pc$ and $M_d = 10^{-3} M_\odot$. The asymmetry was added as one of the 4 types mentioned above.

The major conclusions for the case with $f(r) = 0$ can be drawn from Table 4.1 and Fig. 4.11 to Fig. 4.15. The table summarizes the effect of the asymmetry on $\Delta L_z/L_{z,0}$, which in turn determines the orbit and eccentricity. Fig. 4.11 shows that the torque on the planet due to asymmetric perturbations increases progressively with r_ϵ (provided r_σ is moderately large) and ϵ_0. This is possibly due to the asymmetry influencing more mass of the disk, as total mass in a ring at radius r continues to increase till the scale length. Fig. 4.12 tells that for small r_σ and r_ϵ being near the planet, it doesn't matter on which side of

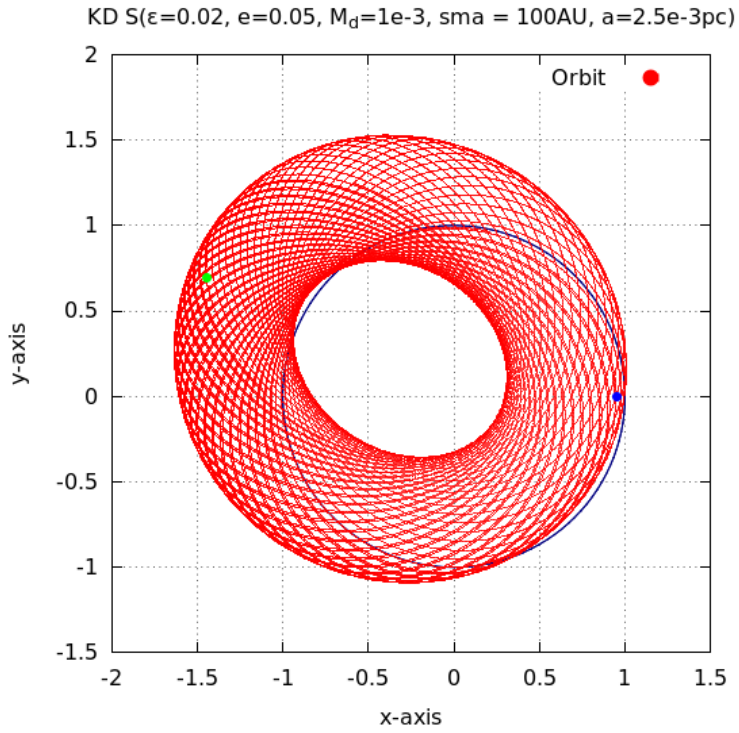

Figure 4.4: Trajectory in embedded asymmetric Kuzmin disk with spiral wave perturbations and constant asymmetry. The thin circle is the unit circle.

Some hints of a shape function are visible. Small circles on the orbit indicate initial and final positions.

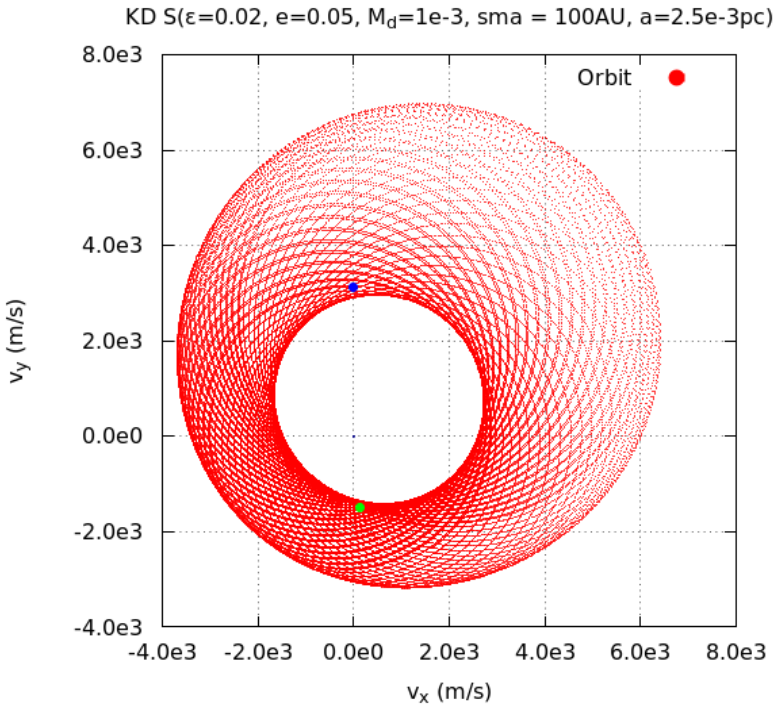

Figure 4.5: Velocity in embedded asymmetric Kuzmin disk with spiral wave perturbations and constant asymmetry.

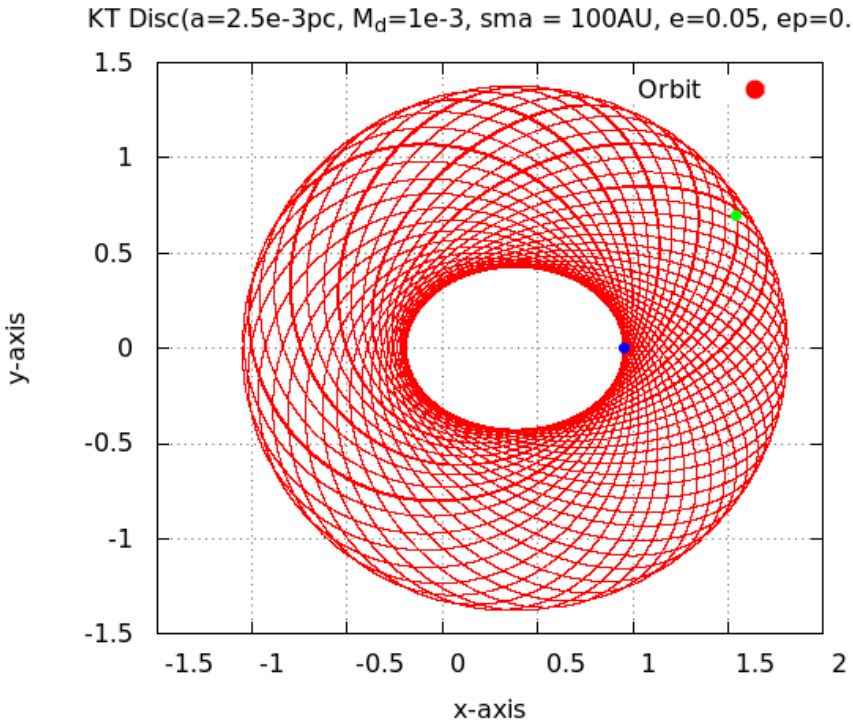

Figure 4.6: Trajectory in embedded asymmetric Kuzmin disk with $f(r) = 0$ and constant asymmetry.

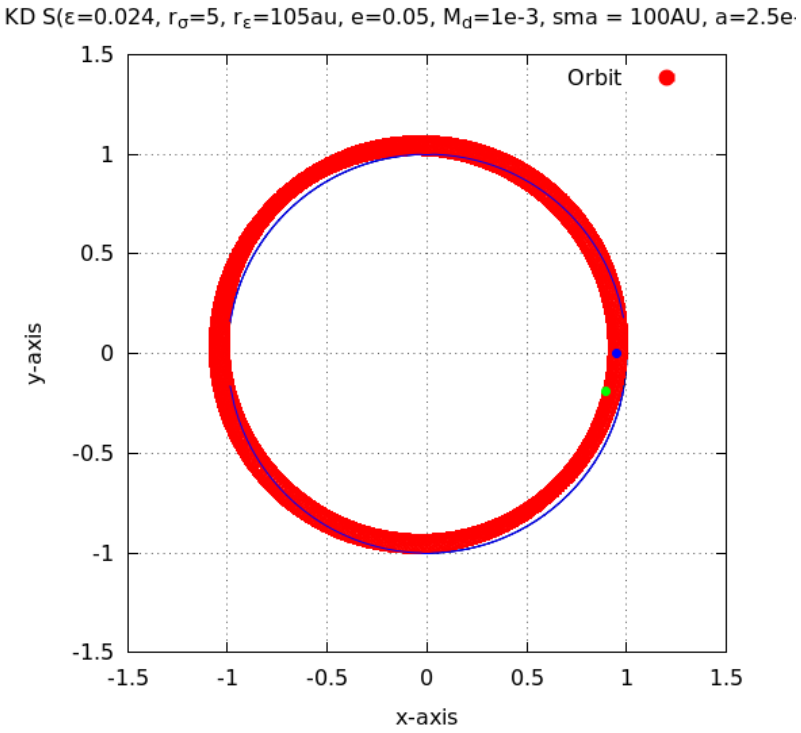

Figure 4.7: Trajectory in embedded asymmetric Kuzmin disk with spiral wave perturbations, $r_\sigma = 5au$, $r_\epsilon = 105au$ and $\epsilon_0 = 0.024$.

the planet the asymmetry peak is located. The torque may even be $+ve$ for small r_σ and $r_\epsilon \neq s.m.a$. The net torque exerted is more for larger r_σ.

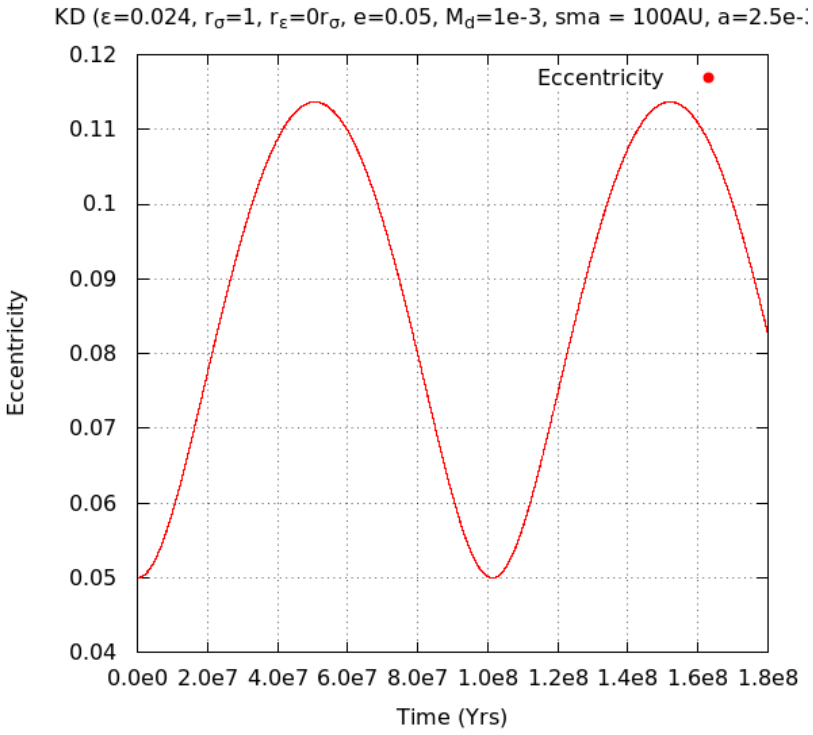

Figure 4.8: Eccentricity in embedded asymmetric Kuzmin disk with $f(r) = 0$, $r_\sigma = 1au$, $r_\epsilon = 100au$ and $\epsilon_0 = 0.024$.

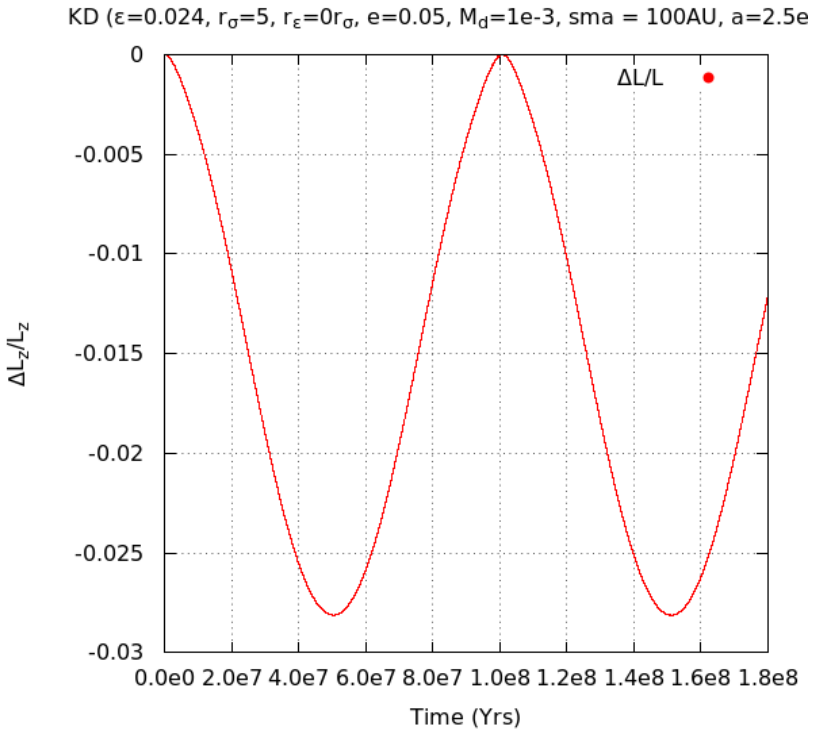

Figure 4.9: $\Delta L_z/L_{z,0}$ in embedded asymmetric Kuzmin disk with $f(r) = 0$, $r_\sigma = 5au$, $r_\epsilon = 100au$ and $\epsilon_0 = 0.024$.

Fig. 4.13 is made for cases such that the integration $\int_0^\infty \epsilon(r)dr = constant$ for the Gaussian asymmetry used. Initial integral was found using $r_\sigma = 5au$ and $r_\epsilon = 100au$,

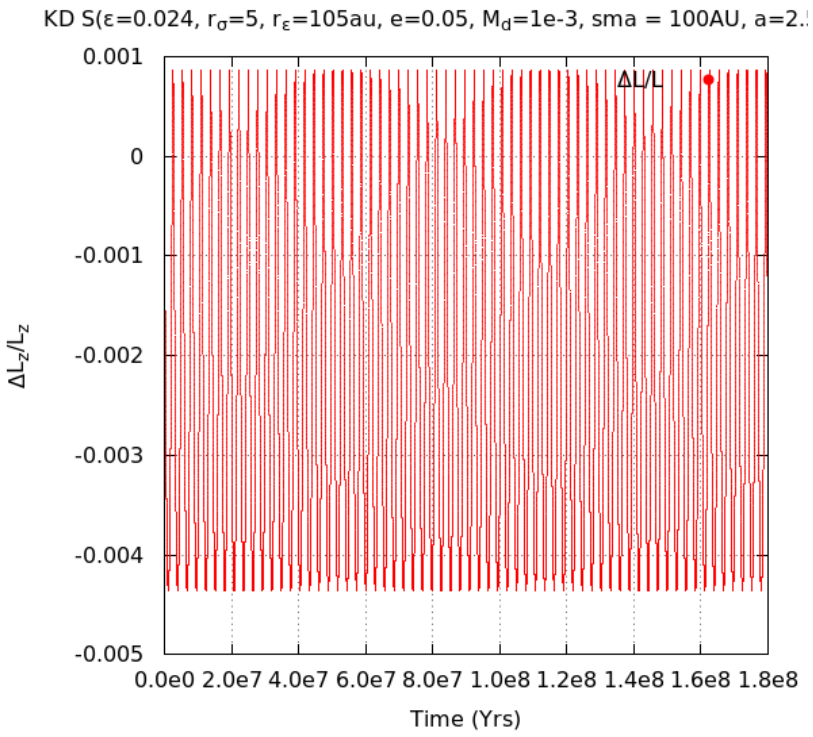

Figure 4.10: $\Delta L_z/L_{z,0}$ in embedded asymmetric Kuzmin disk with $f(r) = \frac{1}{2} log_e\, r$, $r_\sigma = 5au$, $r_\epsilon = 105au$ and $\epsilon_0 = 0.024$.

Notice that the oscillation is not mostly limited to the $+ve$ or $-ve$ side as with the constant ϵ case.

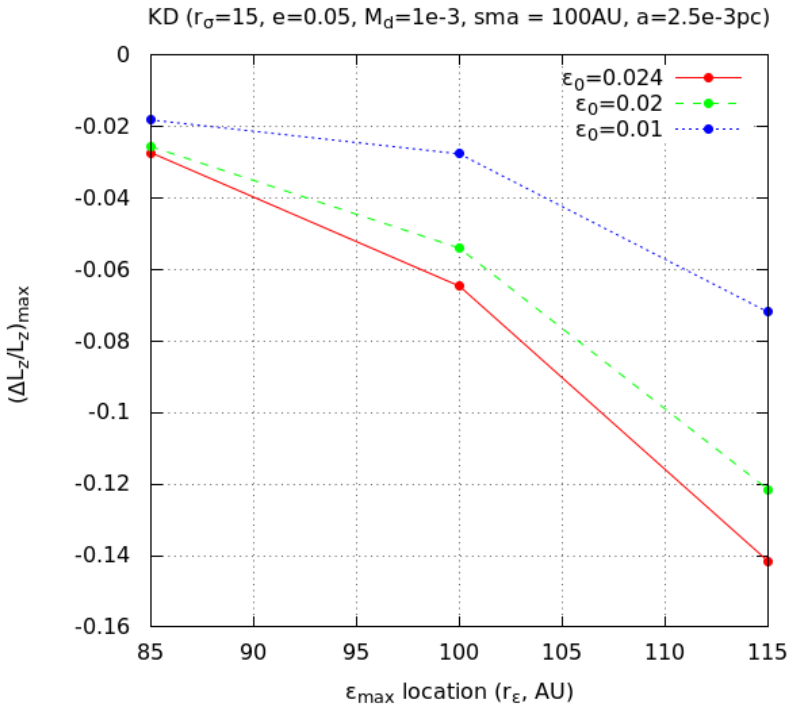

Figure 4.11: $\Delta L_z/L_{z,0}$ vs r_ϵ at $r_\sigma = 15au$ for the Gaussian asymmetry distribution and no shape function.

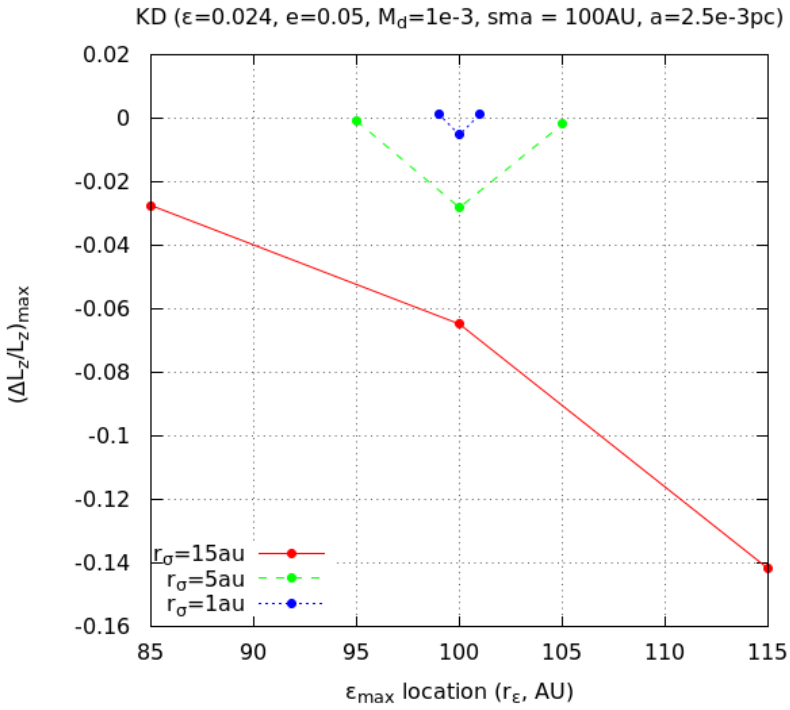

Figure 4.12: $\Delta L_z/L_{z,0}$ *vs* r_ϵ at $\epsilon_0 = 0.024$ for the Gaussian asymmetry distribution and no shape function.

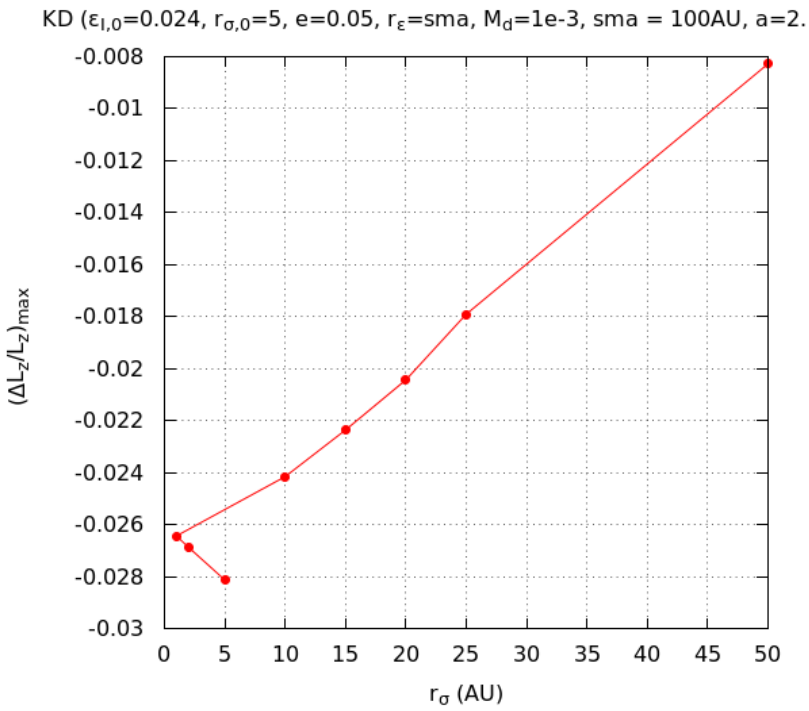

Figure 4.13: $\Delta L_z/L_{z,0}$ *vs* r_σ for the Gaussian asymmetry distribution and no shape function.
The ϵ_0 is found such that the area under the bell curve remains same for all r_σ. The initial area was found using $r_\sigma = 5au$ and $\epsilon_0 = 0.024$.

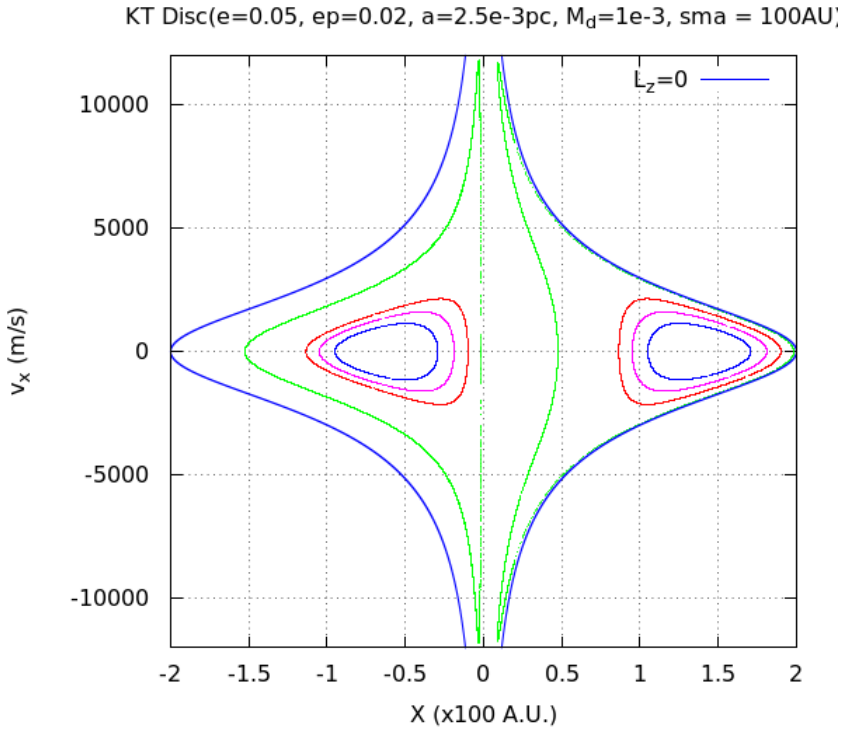

Figure 4.14: Surface of Section (v_x vs x) for added $10^{-3}M_{\odot}$ Kuzmin disk with constant asymmetry, $\epsilon = 0.02$.

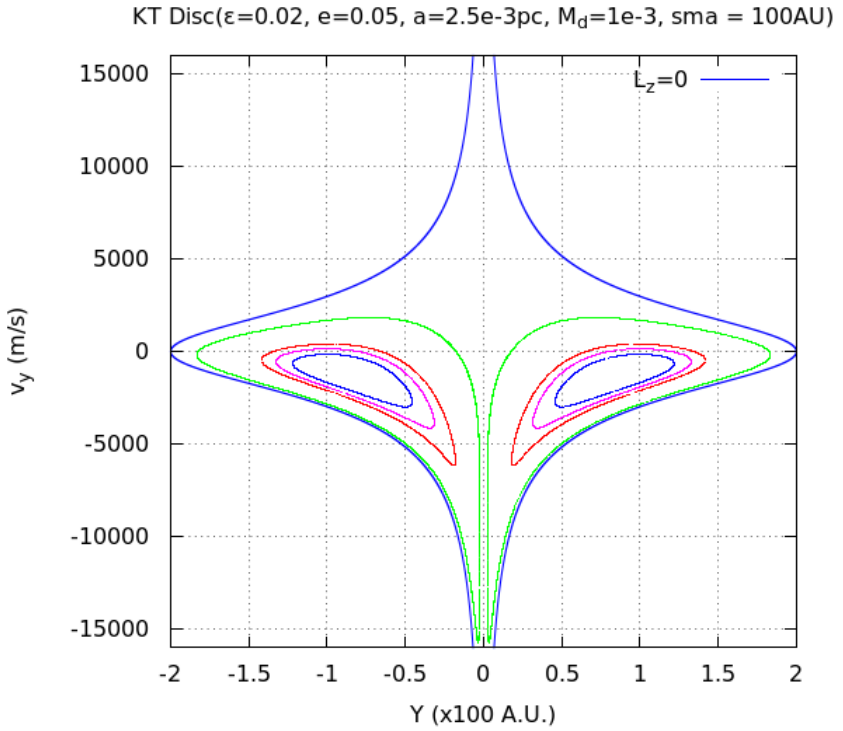

Figure 4.15: Surface of Section (v_y vs y) for added $10^{-3}M_{\odot}$ Kuzmin disk with constant asymmetry, $\epsilon = 0.02$.

which explains why the maximum torque is felt by the planet for $r_\sigma = 5au$. $r_\epsilon = 100au$ was taken to be constant for all cases. For subsequent r_σ (except $5au$), the absolute

magnitude of $\Delta L_z/L_{z,0}$ decreases with increasing r_σ as the asymmetry is being spread over a larger area (and farther from the planet). The case with large r_σ is essentially equivalent to the constant ϵ case with $\epsilon = \epsilon_0$. The SOS plots for $\epsilon = constant$ and $f(r) = 0$ (Fig. 4.14, 4.15) shows that the orbits progressive explore greater range of $L_z/L_{z,0} \in [-1, 0]$ as the asymmetry is increased. This leads to the SOS shift towards the limiting case of $L_z = 0$. Note that the SOS x has shifted from the symmetric case towards the $+ve$ x-axis, where the asymmetry is strongest.

To generalise, nother integral L_z is lost, as now a torque acts on the system. SI4 can till be used as E is still an integral. The planet appears to have its angular momentum oscillate due to the asymmetry. Observations show the angular momentum has a small oscillation over the radial time-period, while a drastic oscillation can be seen over the precession timescale. However, if in the constant ϵ case the asymmetry parameter is too strong the planet will go too near the central star and be possibly ejected or collide (our integrator fails to accurately represent this part) before it can reach its minimum stable inner radius. In fact most cases have $\epsilon = 0.024$ as this was found to be the limiting case for the constant asymmetry.

This case was found to be highly sensitive to the initial conditions, in particular the initial angle of the planet from the direction of maximum asymmetry and the sign of L_z. However, the topology appears to remain the same. Naturally the initial position and velocity are significant in all cases. The spiral wave case has to be investigated further to find patterns in results.

A striking observation is that in most cases the L_z only decreases, with $\Delta L_z/L_z$ never being greater than zero or only being so for a very short duration. There are cases when suitable initial conditions lead to $\Delta L_z/L_z > 0$ throughout the time of the simulation, however the maximum value reached is too small or the r_σ used is small. A possible reason for $\Delta L_z/L_z < 0$ predominantly is the fact that only a very small portion of the mass ($\sim 2\%$) of the disk is inside the orbit of the planet (Equation 3.2) and most of the mass lies well outside the orbit. It is a well established fact that mass inside the orbit typically exerts a positive torque on the body, while it is vice versa for mass outside the orbit[3].

CHAPTER 5

CONCLUSIONS AND FUTURE WORK

The behavior of the system is reasonably well understood till the case where the Kuzmin disk is symmetric. However, there were a varied results upon addition of asymmetric perturbations and it is worth investigating them in detail beyond this present document.

5.1 Epilogue

The presence of a protoplanetary disk greatly alters the orbit of a planet around a host star. The crux of the final orbital structure can be seen as the struggle of the disk to deform the planet orbit to suit itself, while the host star tries to maintain the elliptic path. All cases considered are with static potential, well behaved systems and quasi-periodic orbits.

The traditional Kuzmin disk has no significant topological impact on the orbit if the disk is removed instantaneously. Granted that the orbits do not close upon themselves due to the presence of the disk, but the deviation is not drastic as $\Omega \approx \kappa$. Further there is negligible change in the eccentricity and no change in the semi-major axis. The observations of the simulation can be generalized for different parameters (§3.4). The disk merely facilitates the (slow) precession of the orbit.

5.1.1 Asymmetric Disk

The asymmetric Kuzmin disk, however, has a lot of scope to influence the orbits, especially as L_z no longer is bound to be conserved. Given the choice of parameters, there are manifold possibilities. But it was felt that as the mass fraction contained inside the radius of the orbit is tiny, the full influence of the disk on the orbits was not evident. It will be worthwhile to repeat these exercises at an orbital radius comparable to the scale length or half-mass radius of the disk.

The orbits were again found to be quasi-periodic as the SOS always closes upon itself. A gradual shift of the SOS towards the limiting case ($L_z = 0$) can be seen as the asymmetry is made stronger (Fig. 4.14, 4.15). Also of note is the temptation to label orbital structures for $f(r) = 0$ cases to be a trivial shift of the origin (Fig. 4.6). However, the velocity space is clearly lopsided (similar to Fig. 4.5), indicating the underlying asymmetry. This could also mean that though the position space apparently has a symmetry axis,

the density of crossings at any given area need not be constant. The cases with narrow r_σ, slightly away from the planet's initial orbit were found to reduce the global L_z oscillation timescale by 1 to 2 orders of magnitude! This could be due to the asymmetry mimicking the mass distribution of a heavier Kuzmin disk. However, again the $\Delta L_z/L_{z,0}$ extrema was small.

The cases with spiral wave perturbations have more diverse results. Both the velocity and the phase space give hints of the spiral potential pattern of the disk. Further the angular momentum and eccentricity changes are not limited to either $+ve$ or $-ve$ deviations from the original value, but go both ways.

What remains to be seen and investigated is how these orbital changes may influence the evolution and final structure of planetary systems. Left in its static state, the system would continue to eventually return back to the same configuration over time. Hence, there must be an external potential source or the secular evolution of the disk-star-planet system must be accounted to see any lasting changes. This would albeit make the problem a bit tedious to solve even computationally.

5.2 Future Scope and Recommendations

The problem is still in its early stages, or just a "toy problem."

From the point of view of accuracy, the **indirect potential** [13] on the planet originating from the motion of the host star (the back reaction) due to the presence of the protoplanetary (or debris) disk has to be considered. Also this study considers the gravitational forces to be dominant over other physical effects due to the disk. There is some scope to include hydrodynamical forces. Further, the effect on the planet on the disk cannot be entirely ignored, as the planet can in theory generate drag and spiral wave disturbances in the disk. However, these effect are undoubtedly small enough to be neglected for small, low mass planets.

Most asymmetric disk structures found (galaxies, protoplanetary disk) are found to **rotate** with a characteristic pattern speed Ω_p. This introduces an explicit time dependence on the Hamiltonian in the inertial frame of reference and consequently the Hamiltonian (or the angular momentum) is not conserved. A workaround of this problem is to find the equations of motion in the rotating frame of reference, which have a different form of the Hamiltonian - the **Jacobi Integral** ($\boldsymbol{H_J = H - \Omega \cdot \mathbf{L}}$), which is conserved in the rotating frame. However, this introduces another problem as now the Hamiltonian is non-separable

and the SI4 algorithm is not effective in this case anymore. The *Kustaanheimo-Stiefel* (see [14] [15]) transformation was looked into to solve this problem and it is believed that with some effort it will be possible to apply some form of the symplectic method to this case.

The goal of this study is the seek the mechanism by which protoplanetary disks might lead to migration (especially Type I migration). The protoplanetary disk have a very short lifetime compared to the system as stellar radiation and winds slowly strip away the disk material. As the simulations suggest that the presence of protoplanetary disks lead to orbits which have thick orbital annulus, it would not by impractical to think that the disappearance of the disk midway of the quasi-periodic orbit may freeze the planet at that radius and hence lead to its "migration", though its eccentricity may not be close to zero as statistically desired. However, a time dependence of the mass of the disk would introduce an non-trivial explicit time dependence on the Hamiltonian and it is unlikely that the symplectic formalism can be used that case. Higher order Runge-Kutta methods or Bulirsch-Stoer method would probably have to be sought to study this case. These methods may accumulate errors over the long term evolution and introduce artifacts in the computation.

The last two propositions and the back reaction on the disk are hoped to be accounted in a later study.

REFERENCES

[1] Ernst Hairer, Christian Lubich, and Gerhard Wanner. *Geometric numerical integration*. Springer series in computational mathematics. Springer, New York, 2002.

[2] Michael Perryman. *The Exoplanet Handbook*. Cambridge University Press, 2011.

[3] Philip J. Armitage. *Astrophysics of planet formation*. Cambridge University Press, 2010.

[4] Stephen H. Lubow and Shigeru Ida. Planet migration. *Exoplanets*, 1:347–371, 2010.

[5] H. Kinoshita, H. Yoshida, and H. Nakai. Symplectic integrators and their application to dynamical astronomy. *Celestial Mechanics and Dynamical Astronomy*, 50:59–71, 1991.

[6] H. Yoshida. Recent Progress in the Theory and Application of Symplectic Integrators. *Celestial Mechanics and Dynamical Astronomy*, 56:27–43, 1993.

[7] E. Forest and R. D. Ruth. Fourth-order symplectic integration. *Physica D Nonlinear Phenomena*, 43:105–117, 1990.

[8] David J. D. Earn. Symplectic integration without roundoff error. *Lecture Notes in Physics*, 430:122–130, 1994.

[9] James Binney; Scott Tremaine. *Galactic Dynamics*. Princeton University Press, USA, 2007.

[10] Herbert Goldstein. *Classical mechanics*. Addison-Wesley, Boston, USA, 2000.

[11] S. Tremaine. Slow Modes in Keplerian Disks. *The Astronomical Journal*, 121:1776–1789, March 2001.

[12] D. Lynden-Bell and A. J. Kalnajs. On the generating mechanism of spiral structure. *Monthly Notices of the Royal Astronomical Society*, 157:1, 1972.

[13] J. C. B. Papaloizou. Global m = 1 modes and migration of protoplanetary cores in eccentric protoplanetary discs. *Astronomy and Astrophysics*, 388:615–631, June 2002.

[14] P. Saha. Interpreting the Kustaanheimo-Stiefel transform in gravitational dynamics. *Monthly Notices of the Royal Astronomical Society*, 400:228–231, November 2009.

[15] K. Langner and S. Breiter. Ks variables in rotating reference frame. application to cometary dynamics. *Astrophysics and Space Science*, 357(2):1–10, 2015.

APPENDIX A

SI4 for Added Asymmetric Kuzmin Disk

The FORTRAN 95 code for simulating the evolution and obtaining the surface of section of a planet in the given system can be found below. The system consists of a sun mass star embedded in a asymmetric Kuzmin disk kind of potential with a logarithmic shape function (spiral density profile) and Gaussian distribution of the asymmetry. Note that other cases can be obtained as a limiting case to this potential or by removing the $\log_e(r)$ term.

```
! 4th Order symplectic Method (Forrest-Ruth Algorithm) for
   Kuzmin disc with asymmetric factor

program forest_ruth
   implicit none
   real(kind = 8), parameter :: year = 3.1556926d7, ms=1.989d30,
       me=5.973d24
   ! Seconds in years, Mass of sun, Mass of Earth
   real(kind = 8), parameter :: PI = 3.14159265358979323d0, G
      =6.67408d-11
   real(kind = 8), parameter :: lda = 1.35120719195965763d0, pc
      =3.085677581d16
   ! SI4 constant, Parsec in meter
   real(kind=8), parameter :: rc=G*ms/256d6, vc=16d3, tc=rc/vc
   ! Scales to make quantities dimensionless
   ! Taking $ G M_\odot t_c^2=r_c^3. \ and \ v_c = 16d3 $
   real(kind = 8), parameter :: mr = ms/me, au = 1.496d11
   ! Mass Ratio, Astronomical Unit
   real(kind = 8), parameter :: leng = 2.5d-3*pc/rc, sma = 100*
      au, ec = 5d-2
   ! Length Scale, Semi-Major Axis, Eccentricity
   real(kind = 8), parameter :: ls2 = leng**2, mew = G*ms, cl1=
      rc/sma*1.0
   ! Some derived constants
   real(kind = 8), parameter :: md = 1d-3, ep0 = 2.4d-2
   ! Mass of Disc, Pattern Speed, Asymmetry parameter
   real(kind = 8), parameter :: r_s=5d0*au/rc, r_ep=sma/rc,
      r_s_2in=r_s**(-2)
   ! Std Dev of Radius, Peak, Variance(Gaussian type asymmetry)
!  real(kind = 8), parameter :: r_s=1d38*au/rc, r_ep=0, r_s_2in=
   r_s**(-2)
   integer, parameter :: D1=2, D2=2 ! No. of bodies, Dimensions
   real(kind=8),parameter :: dt=year*1d-1/tc,tt=1.8e8*year/tc
   ! Time step, Total Time
```

```
real(kind = 8) :: x(D1,D2), v(D1,D2), a(D1,D2), t=0d0
! Motion elements for Star(1), Planet(2) (All =0 for Star);
   Initial time
real(kind = 8) :: prev(D2+2), tl(2), st0, sqdci, r2, rin, ri3
   , r , csp, snp
! Temporary variable to store or optimize
integer :: i=0, j, samp=nint(180*year/tc/dt) !, flag=0 ! samp
    is sampling interval
real(kind = 8) :: L02, L2, E02, e2, ep, tor
! L2 & E2 = Angular Momentum & Energy of planet; tor=Torque
real(kind = 8) :: c(4), d(3), om, kp, pr, tol, ratio, ecc(D2)
! c, d: SI4 constants; Variable for disk parameters

x(2,:) = [ sma*(1d0-ec)/rc, 0.0d0/rc ] ! Perigee
x(1,:) = 0
v(2,:) = [0d0, sqrt(mew*(2d0/(sma*(1d0-ec))-1d0/sma))/vc] !
   vis-viva eqn
v(1,:) = 0

c = [ 0.5d0*lda, 0.5d0*(1.0d0-lda), 0.5d0*(1.0d0-lda), 0.5d0*
   lda ]
d = [ lda, 1.0d0-2.0d0*lda, lda ]
tol = 4d-5/rc*sma ! Tolerance for SoS

om = sqrt(mew*(sma**(-3) + md*sqrt((sma*sma+ls2*rc*rc)**(-3))
   ))*year
kp = sqrt(mew*(sma**(-3) + md*(sqrt(sma*sma+ls2*rc*rc)**(-5))
   *(4*ls2*rc*rc+sma*sma)))*year
pr = om - kp

write(*,*) "om=", om, 2*PI/om, "kp=", kp, 2*PI/kp, "pr=", pr,
    2*PI/pr
write(*,*) "v_c =", om/year*sma, st0, samp
write(*,*) "Gauss=", r_s*rc/au, r_ep*rc/au, (r_s*rc/au)**(-2)

open(11, file='spiral/frks8-1e.05_3N.024_5.txt')
! f = Forest-Ruth, k = KT Disc, s=spiral, e= eccentricity, _3
   =disc_mass, N=Normal_Distribution, .024=ep0, 5 -> r_s
open(13, file='spiral/frks8-1e.05_3N.024_5ssy.txt')
open(12, file='spiral/frks8-1e.05_3N.024_5ssx.txt')

write(11,*) "# a=", leng, "ecc=", ec, "M_d=", md
write(11,*) "# om=", om, 2*PI/om, "kp=", kp, 2*PI/kp, "pr=",
   pr, 2*PI/pr
write(11,*) "# Bulge: ep_0", ep0, "r_s=", r_s*rc/au, "r_ep=",
    r_ep*rc/au

tl(1) = 2.5d5*tp/tc
tl(2) = tt-tl(1)
r2 = sum(x(2,:)**2)
r = sqrt(r2)
```

```
   ep = ep0*exp(-r_s_2in*((r-r_ep)**2))
   rin = 1.0d0/r
   !***************** cos(atan2(y,x)) = x/r ****************
   csp = cos(atan2(x(2,2),x(2,1))-0.5*log(sqrt(r2)))
   E02 = -rin + 0.5d0*sum(v(2,:)**2) - md*(1d0+ep*csp)/sqrt(r2+
      ls2)
   L02 = x(2,1)*v(2,2) - x(2,2)*v(2,1)
   write(11,*) "# E=", E02, "L_z=", L02
   write(*,*) -rin, 0.5d0*sum(v(2,:)**2), - md*(1d0+ep*x(2,1)*
      rin)/sqrt(r2+ls2)

   !***Changing initial condition (L_z) keeping E constant***
   x(2,:) = [ sma*(1d0-ec)/rc, 0.0d0 ]
   r2 = sum((x(2,:))**2)
   csp = cos(atan2(x(2,2),x(2,1))-0.5*log(sqrt(r2)))
   write(11,*) "# x(2,:) = [ sma*(1d0-ec)/rc, 0.0d0 ] "
   st0 = E02 + 1d0/sqrt(r2) + md*(1d0+ep*csp)/sqrt(r2+ls2)
   if(st0 < 0) write(*,*) "Unphysical"
   st0 = sqrt(2d0*st0)
   v(2,:) = [ 0d0, st0 ]
   L02 = x(2,1)*v(2,2) - x(2,2)*v(2,1)
   write(*,'(4g13.5)') x(2,:)*cl1, v(2,:)*vc
   write(11,*) "# E=", E02, "L_z=", L02

   write(*,*) "dt = ", dt, "rc = ", rc, "T_p = ", tp/year
   prev = [x(2,1), x(2,2)+1d-15, v(2,1), v(2,2)]
   st0 = x(2,2)

   do while(t<=tt)
      if(i==samp) i=0
      ! ~60 points/orbit needed for good ellipse
      if( i==0 ) then
   ! Only every {samp}^th value is recorded due to memory limits
         r2 = sum(x(2,:)**2)
         r = sqrt(r2)
         ep = ep0*exp(-r_s_2in*((r-r_ep)**2))
         rin = 1.0d0/r
         sqdci = 1d0/sqrt(r2+ls2)
         csp = cos(atan2(x(2,2),x(2,1))-0.5*log(sqrt(r2)))
         e2 = -rin + 0.5d0*sum(v(2,:)**2) - md*(1d0+ep*csp)/sqrt
            (r2+ls2)
         L2 = x(2,1)*v(2,2) - x(2,2)*v(2,1)
! Alternate:ecc = (sum(v(2,:)**2)-rin)*x(2,:)-v(2,:)*(x(2,1)*v
   (2,1)+x(2,2)*v(2,2))
         ecc = L2*[v(2,2),-v(2,1)]-x(2,:)*rin
         ratio = atan2(ecc(2), ecc(1))
         ecc = [sqrt(sum(ecc**2)), ratio]
         tor = -md*ep*x(2,2)*rin*sqdci
         write(11,'(11g13.5)') x(2,:)*cl1, t*tc/year, e2/E02
            -1.0, v(2,:)*16d3, L2/L02-1.0, ecc, tor
      end if
```

```
!****This block finds the surface of section with y=0*****
   if( (x(2,2)*prev(2) .le. 0) ) then
      if( (abs(x(2,2))+abs(prev(2))<tol) .and. (abs(prev(2))
         > 0) ) then
         ratio = abs(x(2,2))/abs(prev(2))
         write(12,'(3g15.7, 1g13.5)') (x(2,1)+ratio*prev(1))*
            cl1/(ratio+1), &
            (v(2,1)+ratio*prev(3))*16d3/(ratio+1), x(2,2)*cl1
               , t*tc/year
      else if( abs(x(2,2))<tol/4 ) then
         write(12,'(3g15.7, 1g13.5)') x(2,1)*cl1, v(2,1)*16d3
            , x(2,2)*cl1, t*tc/year
      else if( abs(prev(2))<tol/4 ) then
         write(12,'(3g15.7, 1g13.5)') prev(1)*cl1, prev(3)*16
            d3, prev(2)*cl1, t*tc/year
      end if
   end if

!****This block finds the surface of section with x=0*****
   if( (x(2,1)*prev(1) .le. 0) ) then !combine both
      if( (abs(x(2,1))+abs(prev(1))<tol) .and. (abs(prev(1))
         > 0) ) then
         ratio = abs(x(2,1))/abs(prev(1))
         write(13,'(3g15.7, 1g13.5)') (x(2,2)+ratio*prev(2))*
            cl1/(ratio+1), &
            (v(2,2)+ratio*prev(4))*16d3/(ratio+1), x(2,1)*cl1
               , t*tc/year
      else if( abs(x(2,1))<tol/4 ) then
         write(13,'(3g15.7, 1g13.5)') x(2,2)*cl1, v(2,2)*16d3
            , x(2,1)*cl1, t*tc/year
      else if( abs(prev(1))<tol/4 ) then
         write(13,'(3g15.7, 1g13.5)') prev(2)*cl1, prev(4)*16
            d3, prev(1)*cl1, t*tc/year
      end if
   end if
   prev = [x(2,1), x(2,2), v(2,1), v(2,2)]

!**************Main loop of SI4 algorithm*****************
   do j=1, 4, 1
      x(2,:) = x(2,:) + c(j)*dt*v(2,:)
      if(j==4) exit

      r2 = sum(x(2,:)**2)
      r = sqrt(r2)
      ep = ep0*exp(-r_s_2in*((r-r_ep)**2))
      rin = 1.0d0/r
      ri3 = rin*rin*rin
      sqdci = 1d0/sqrt(r2+ls2)
      snp = atan2(x(2,2),x(2,1))-0.5*log(sqrt(r2))
      csp = cos(snp)
```

```
            snp = sin(snp)

            a(2,1) = -ri3*x(2,1) + ep*md*snp*sqdci*(x(2,2)+0.5*x
               (2,1))/r2 &
               - 2d0*md*(r-r_ep)*r_s_2in*ep*x(2,1)*rin*csp*sqdci &
               - md*x(2,1)*(1d0+ep*csp)*(sqdci**3)
            a(2,2) = -ri3*x(2,2) - ep*md*snp*sqdci*(x(2,1)-0.5*x
               (2,2))/r2 &
               - md*2d0*(r-r_ep)*r_s_2in*ep*csp*x(2,2)*rin*sqdci &
               - md*x(2,2)*(1d0+ep*csp)*(sqdci**3)
            v(2,:) = v(2,:) + d(j)*dt*a(2,:)
         end do
         t = t+dt
         i = i+1
      end do
      close(11); close(12); close(13)
end program forest_ruth

! * Compile/Execute Commands
! * gfortran fr_kt_fx_asym_er_gs.f95 -O3 -ffast-math
! * time ./a.out
! * Gnuplot is used for plotting
```